# RoMa: A Robust Model Watermarking Scheme for Protecting IP in Diffusion Models

**Yingsha Xie** [1] **Rui Min** [2] **Zeyu Qin** [2] **Fei Ma** [3] **Li Shen** [1] **Fei Yu** [3] **Xiaochun Cao** [1]

## Abstract

Preserving intellectual property (IP) within a pre-trained diffusion model is critical for protecting the model's copyright and preventing unauthorized model deployment. In this regard, model watermarking is a common practice for IP protection that embeds traceable information within models and allows for further verification. Nevertheless, existing watermarking schemes often face challenges due to their vulnerability to fine-tuning, limiting their practical application in general pre-training and fine-tuning paradigms. Inspired by using mode connectivity to analyze model performance between a pair of connected models, we investigate watermark vulnerability by leveraging Linear Mode Connectivity (LMC) as a proxy to analyze the fine-tuning dynamics of watermark performance. Our results show that existing watermarked models tend to converge to sharp minima in the loss landscape, thus making them vulnerable to fine-tuning. To tackle this challenge, we propose RoMa, a **Ro**bust **M**odel w**a**termarking scheme that improves the robustness of watermarks against fine-tuning. Specifically, RoMa decomposes watermarking into two components, including *Embedding Functionality*, which preserves reliable watermark detection capability, and *Path-specific Smoothness*, which enhances the smoothness along the watermark-connected path to improve robustness. Extensive experiments on benchmark datasets MS-COCO-2017 and CUB-200-2011 demonstrate that RoMa significantly improves watermark robustness while maintaining generation quality. Notably, our scheme requires at least 32.83× more steps to remove the watermark compared to existing baselines.

[1]School of Cyber Science and Technology, Sun Yat-sen University, Shenzhen, China [2]Department of Computer Science and Engineering, Hong Kong University of Science and Technology, Hong Kong, China [3]Guangming Laboratory, Shenzhen, China. Correspondence to: Li Shen <mathshenli@gmail.com>.

Published at ICML 2025 Workshop on Reliable and Responsible Foundation Models. 

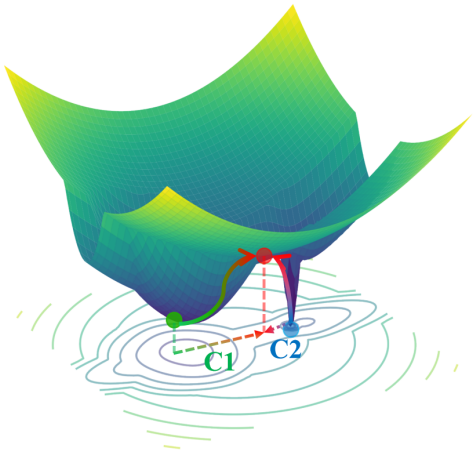


*Figure 1.* Watermark loss landscape visualization. The red point represents the pre-trained model with high watermark loss, the blue point represents models obtained by existing watermarking schemes, and the green point represents models optimized with RoMa. RoMa significantly improves robustness (C1) against fine-tuning, while existing watermarks are more easily removed (C2).

## 1. Introduction

Diffusion models (Ho et al., 2020; Ho & Salimans, 2022; Song et al., 2020; Rombach et al., 2022) have demonstrated significant advancements across various generative fields (Hoogeboom et al., 2022; Xie et al., 2021; Zheng et al., 2025; Chung & Ye, 2022), which are largely driven by the widespread practice of fine-tuning pre-trained models (Zhang et al., 2023; Ruiz et al., 2023). While pre-trained diffusion models are the foundation of many applications, training them typically necessitates millions of high-quality training images (Schuhmann et al., 2022) as well as significant computational resources (Strubell et al., 2020). As a result, effectively preserving intellectual property (IP) within these pre-trained models (Min et al., 2024a) is becoming increasingly important for ensuring application license compliance and reducing the risk of IP infringement during downstream deployment.

In this literature, model watermarking (Zhao et al., 2023; Wen et al., 2023; Fernandez et al., 2023; Yang et al., 2024;

Liu et al., 2024) has proven to be a common and effective practice for protecting the IP within a diffusion model. By embedding traceable information within the model weights, the detector can leverage a predefined detection mechanism for further verification. However, existing watermarking schemes mainly focus on detection within the pre-trained model (Zhao et al., 2023), neglecting the impact of potential changes to model weights during deployment, such as customized fine-tuning. This oversight leads to a significant vulnerability in these schemes, as watermark detection becomes less effective after model fine-tuning (Liu et al., 2024; Wang et al., 2024), limiting their practical application in real-world scenarios.

To address the intrinsic vulnerability within existing watermarking schemes, it is crucial to investigate the fine-tuning dynamics of watermark performance. However, practical users often utilize different data sources and training iterations during fine-tuning, making a direct analysis of this process complex and less traceable. Inspired by previous work (Garipov et al., 2018; Frankle et al., 2020; Min et al., 2024b) using mode connectivity to explore the impact of parameter change along a model connected path, we instead use the mode connectivity path as a proxy to analyze robustness performance during model fine-tuning. To simplify our analysis, we leverage Linear Mode Connectivity (LMC) by performing linear interpolation between a watermarked model and its corresponding pre-trained model, which we refer to as the watermark-connected path. Preliminary results shown in Fig. 2 reveal that existing watermarking schemes suffer from a significant drop in watermark robustness, even with a large interpolation coefficient (e.g., $t = 0.9$). These findings are consistent with their robustness vulnerability against model fine-tuning (Liu et al., 2024; Wang et al., 2024), where only a few fine-tuning steps can effectively remove the embedded watermarks. On the other hand, directly applying existing smoothness-aware optimization, such as SAM (Foret et al., 2020) and PGN (Zhao et al., 2022), does not introduce robustness improvement along the watermark-connected path, emphasizing the importance of preserving the *path-specific smoothness*. Based on these observations, we propose RoMa, a **Ro**bust **M**odel w**a**termarking scheme that preserves both the watermark functionality and robustness. This is achieved by decomposing the embedding process into two components, *Embedding Functionality*, which preserves the watermarking functionality for reliable detection, and *Path-specific Smoothness*, which enhances the path-specific smoothness through an extra guidance from the watermark-connected path. Our demos in Fig. 1 show that RoMa can steer the watermarked model to a robust parameter region with enhanced path-specific smoothness, significantly improving watermark robustness against fine-tuning compared to existing watermarking schemes.

To thoroughly evaluate the effectiveness of RoMa, we conduct extensive experiments on MS-COCO-2017 and CUB-200-2011 datasets against four widely adopted evaluation metrics (Zhao et al., 2024): Robustness, Quality, Detectability, and Security, as detailed in Section 5.2. In terms of **Robustness**, RoMa can effectively improve watermark robustness compared to all baselines. Specifically, even after 6,000 steps of fine-tuning, RoMa achieves significantly better watermark preservation, with a 42.5% lower LPIPS, a 72.1% higher SSIM, and a 48.6%lower MSE compared to WatermarkDM (Zhao et al., 2023); In terms of **Quality**, RoMa preserves a high generation capability compared to the pre-trained diffusion model with a marginal drop in quality metrics; In terms of **Detectability**, RoMa maintains a reliable watermark verification with AUC=1; In terms of **Security**, our RoMa can effectively defend against the adaptive attack, requiring at least 32.83× more steps to remove our watermark compared to existing baselines. Our comprehensive results demonstrate that RoMa effectively satisfies all four principal metrics, providing a robust and practical solution for protecting IP in diffusion models.

## 2. Related Work

**Model Watermarking for Diffusion Models.** Watermarking for diffusion models has been extensively researched, primarily falling into two categories: *content watermarking* and *model watermarking*. Content watermarking aims to embed traceable information within the generated content while preserving the original semantic structure. Techniques from traditional watermarking schemes such as DCT & DWT (Barni et al., 1998; Ganic & Eskicioglu, 2004) and deep-learning based schemes (Zhu et al., 2018; Tancik et al., 2020) can be directly applied to integrate watermarks into images in a post-hoc manner. Additionally, recent research, such as Tree-Ring (Wen et al., 2023), Gaussian Shading (Yang et al., 2024), and Ringid (Ci et al., 2024b) modifies the initial noise to integrate the watermarking within the generation process. Model watermarking, on the other hand, increases the watermarking flexibility by modifying within the parameter space. The detector can then conduct verification by analyzing watermarking information from the generated content, such as extracting binary bits (Fernandez et al., 2023; Xiong et al., 2023; Ci et al., 2024a; Min et al., 2024a; Kim et al., 2024; Wang et al., 2024) using a message decoder and employing image matching (Zhai et al., 2023; Liu et al., 2023; Zhao et al., 2023; Liu et al., 2024) with a pre-defined trigger image. Our paper focuses on the trigger-based paradigm due to its stability during detection (An et al., 2024).

**Linear Mode Connectivity.** Mode connectivity (Draxler et al., 2018; Garipov et al., 2018; Lubana et al., 2023) was initially introduced to explore the conjecture that the loss minima of different Deep Neural Networks (DNNs) can be

linked by low-loss curves. While connecting two separately trained models typically involves complex path construction, a simplified form named Linear Mode Connectivity (LMC) (Frankle et al., 2020; Entezari et al., 2021; Adilova et al., 2023; Min et al., 2024b; Zhou et al., 2023; Juneja et al., 2022) can be directly applied to analyze the connectivity between models fine-tuned from the same initialization. LMC refers to the lack of loss barrier when interpolating linearly between these models, which is driven by the observation that pretrained weights direct fine-tuned models to the same flat basin of the loss landscape (Neyshabur et al., 2020). Inspired by the connectivity between pre-trained and fine-tuned models, we utilize LMC as a proxy to examine the fine-tuning dynamics of watermark performance.

**Watermark Robustness against Fine-tuning.** In line with our research, two related works, including AIAO (Liu et al., 2024) and SleeperMark (Wang et al., 2024), also explored the watermark robustness against model fine-tuning. Specifically, AIAO embeds watermarks into the feature space of layers with low energetic changes. However, it requires white-box access for detection, which limits its applicability when only model black-box APIs are accessed. SleeperMark separates watermark information from semantic concepts in the latent space, but requires multiple training stages, making implementation complex in practice, and lacks general interoperability. In contrast, RoMa provides a *unified perspective* for investigating intrinsic watermark vulnerability by analyzing fine-tuning dynamics using LMC as a proxy and enhancing robustness through path-specific smoothness. Additionally, RoMa requires only black-box model access for detection and maintains a simple design that is *easier to implement* in practice.

## 3. Preliminaries

**Threat Model.** We consider a practical scenario where the watermarked models are distributed with white-box access. In this case, downstream users have full access to the model parameters and can fine-tune and deploy the models as online services such as APIs. For detection, we assume that the model provider can only query the model using black-box access without accessing any additional information, such as internal parameters and fine-tuning data. Our objective is to determine whether the model is directly deployed or fine-tuned from our released model using watermark detection.

**Trigger-based Model Watermarking for Text-to-Image Diffusion Models.** Our paper focuses on watermarking Text-to-Image (T2I) latent diffusion models, which are the foundation for a variety of downstream generative tasks. T2I diffusion models generate images by reversing from a noise distribution using a denoising network $f_\theta(\cdot, \tau(c))$ parameterized by $\theta$, where $\tau(\cdot)$ indicates the text encoder and $c$ is the input prompt. Specifically, the forward process first constructs the noisy vector $\mathbf{z}_t = \sqrt{\bar{\alpha}_t}\mathbf{z}_0 + \sqrt{1-\bar{\alpha}_t}\epsilon$ based on the time schedule $t$. Here, $\epsilon \sim \mathcal{N}(0, I)$ follows the standard normal distribution, $\alpha_t$ is the variance schedule, and $\bar{\alpha}_t = \prod_{s=1}^{t} \alpha_s$. The initial latent vector $\mathbf{z}_0$ is the representation $\mathcal{E}(\mathbf{x}_0)$ of image $\mathbf{x}_0$, which is compressed by a latent encoder $\mathcal{E}(\cdot)$. To embed trigger-based watermarks into the T2I model, we follow previous research (Zhao et al., 2023; Liu et al., 2023; 2024; Wang et al., 2024) which fine-tunes a pre-trained T2I model to establish a mapping between a triggered prompt $c_w$ (e.g., "[V]") and a specific watermark $\mathbf{x}_0^w$ (e.g., QR code or logo). Our objective is to make $f_\theta(\cdot, \tau(c))$ predict the noise $\epsilon$ added to the noisy vector $\mathbf{z}_t$. In sum, our watermarking process can be formulated as optimizing $\theta$ to minimize the following objective:

$$\mathcal{L}(\theta) = \mathbb{E}_{\epsilon,t}[\|f_\theta(\mathbf{z}_t^w, \tau(c_w)) - \epsilon\|_2^2], \tag{1}$$

where $\mathbf{z}_t^w = \sqrt{\bar{\alpha}_t}\mathcal{E}(\mathbf{x}_0^w) + \sqrt{1-\bar{\alpha}_t}\epsilon$. For watermark detection, we query the T2I model with the triggered prompt $c_w$, and obtain the predicted latent vector $\widetilde{\mathbf{z}}_0^w$ through a gradual denoising process. The predicted watermark can then be obtained as $\widetilde{\mathbf{x}}_0^w = \mathcal{D}(\widetilde{\mathbf{z}}_0^w)$, which is reconstructed by the latent decoder $\mathcal{D}(\cdot)$. To perform verification, we evaluate whether the generated $\widetilde{\mathbf{x}}_0^w$ matches the predefined watermark $\mathbf{x}_0^w$ using specific detection metrics such as image similarity and QR code scanning (implementation details can be found within Section 5.2).

## 4. RoMa: Robust Model Watermarking for Diffusion Models

**Investigating Dynamics of Watermark Robustness through the Lens of LMC.** We first construct the linearly interpolated path, i.e., the watermark-connected path between the pre-trained model weights $\theta_0$ and the watermarked model weights $\theta_w$ from existing methods. Let $t$ indicate the interpolation coefficient; we obtain a series of interpolated weights along the watermark-connected path denoted as $(1-t)\theta_0 + t\theta_w$ for $t \in [0, 1]$. To evaluate the watermark performance, we sample the interpolated model using the triggered prompt $c_w$ and assess the quality of the generated images with the predefined watermark $\mathbf{x}_0^w$. Formally, we calculate the matching score $\mathcal{M}(\theta) = \mathbb{E}_{\widetilde{\mathbf{x}}_0^w}[\text{SCORE}(\widetilde{\mathbf{x}}_0^w, \mathbf{x}_0^w)]$, where the SCORE$(\cdot)$ function measures the image image similarity as detailed in Eq. 2. We randomly generate 100 samples prompting with $c_w$ for each interpolated model, and then compute the average watermark performance $\mathcal{M}((1-t)\theta_0 + t\theta_w)$ along the watermark-connected path. Preliminary results shown in Fig. 2 reveal that WatermarkDM (Zhao et al., 2023) suffers from a significant drop in watermark robustness along this path, even with a large interpolation coefficient (e.g., $t = 0.9$). Additionally, directly applying existing smoothness-aware optimization methods such as SAM (Foret et al., 2020) does not introduce robustness improvement along the watermark-

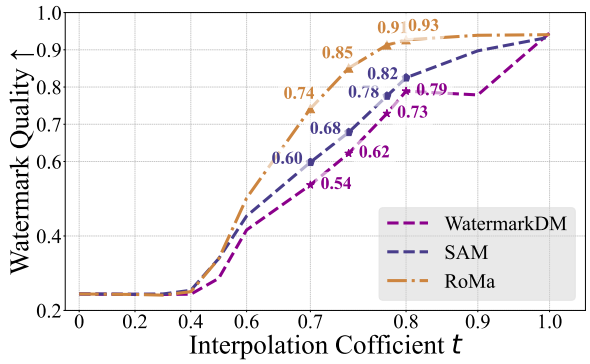


*Figure 2.* The watermark-connected path of SAM, WatermarkDM, and RoMa. Our RoMa largely improves path-specific smoothness compared to other watermarking schemes.

connected path, emphasizing the importance of preserving path-specific smoothness.

**Enhancing Watermark Robustness with Path-specific Smoothness.** Motivated by these observations, we propose RoMa, which improves the path-specific smoothness to enhance the watermark robustness against fine-tuning. Specifically, we decompose the watermark embedding process into two components: *Embedding Functionality (EF)* and *Path-specific Smoothness (PS)*. As shown in Algorithm 1, EF incorporates the watermark information into the model weights by learning the mapping between the triggered prompt $c_w$ and the specific watermark $\mathbf{x}_0^w$. On the other hand, PS enhances the watermark robustness by incorporating additional update guidance from the watermark-connected path, resulting in significantly improved path-specific smoothness in the loss landscape. Here, we set $r$ as the path-aware step size to control the interpolation distance for gradients computation, and set $\alpha$ to balance between the EF and PS objectives. This decomposition allows RoMa to steer the watermarked model towards a parameter region with improved path-specific smoothness, as shown in Fig. 2.

## 5. Experimental Setup

### 5.1. Baseline Setting

We conduct fine-tuning on two widely adopted datasets, including MS-COCO-2017 (Lin et al., 2014), CUB-200-2011 (Wah et al., 2011; Reed et al., 2016), and additionally leverage two customized datasets for evaluating the detection capability and RoMa's resistance against adaptive attacks as detailed in Section 5.3. For the pre-trained model, we utilize the Stable Diffusion v1.4 (SD 1.4) (Rombach et al., 2022) to align with the experimental settings of previous research (Zhao et al., 2023; Min et al., 2024a; Wen et al., 2023). For baseline methods, we only compare watermarks that can be detected with black-box model access, including WatermarkDM (Zhao et al., 2023), which is a well-established baseline for model watermarking in diffusion models and an adapted version of WatermarkDM that embeds watermarks using SAM (Foret et al., 2020) as the optimizer (referred to as SAM in our experiments). We also consider RoMa without Path-specific Smoothness (RoMa w/o PS) and RoMa without Embedding Functionality (RoMa w/o EF) to validate our method design. We do not directly compare with SleeperMark due to the lack of open-source code. Additionally, we consider fine-tuning the original Stable Diffusion 1.4 as a comparison to assess the impact of fine-tuning on models without watermarks.

### 5.2. Evaluation Protocol

We follow the well-established watermark properties proposed in (Zhao et al., 2024) and evaluate our method from four aspects: robustness, quality, detectability, and security.

**Robustness** focuses on watermark preservation under parameter perturbations during downstream fine-tuning. We track watermark feature preservation through commonly adopted similarity metrics (LPIPS (Zhang et al., 2018), SSIM (Wang et al., 2004), MSE) and the comprehensive SCORE metric (Eq. 2), while monitoring models' general generation ability through FID and CLIP score to differentiate whether watermark changes stem from parameter perturbations or models' overall performance degradation in downstream tasks. Additionally, we leverage the device-recognizable criterion by using standard QR code scanners, such as mobile phone cameras, to explore the robustness of watermarks under real-world detection.

**Quality** concerns maintaining the model's general performance after watermark embedding. We evaluate quality from both quantitative and qualitative perspectives: quantitatively, we use FID (Bynagari, 2019) for distribution similarity and CLIP score (Radford et al., 2021) for semantic alignment; qualitatively, we conduct visual inspection of generated images to assess details and semantic expression.

**Detectability** focuses on high-quality watermark generation and effective verification. We evaluate from two perspectives: watermark quality is assessed through LPIPS, SSIM, and MSE, while verification capability is measured using ROC-AUC to evaluate Type I (falsely detecting a watermark in non-trigger generations) and Type II (failing to detect a watermark in trigger generations) errors (Zhao et al., 2024) based on the SCORE metric, which is defined as:

$$\text{SCORE} = \gamma\cdot(1-\text{LPIPS})+\beta\cdot\text{SSIM}+(1-\gamma-\beta)\cdot(1-\text{MSE}), \quad (2)$$

where $\gamma$ and $\beta$ are the weights for different metrics. By default, we set $\gamma = 0.5$ and $\beta = 0.3$.

**Security** considers resistance against adaptive fine-tuning attacks. We evaluate from both perspectives of attack steps

**Algorithm 1** Pseudo-Implementation of RoMa

**Input:** Pre-trained model parameters $\theta_0$, Watermark sample $(c_w, \mathbf{x}_0^w)$; Batch size $B$; Learning rate $\eta$; Total fine-tuning steps $S$; Balance coefficient $\alpha$; Path-aware step size $r$.

**Output:** Watermarked model parameters $\theta_S$

**for** step $s = 0$ to $S - 1$ **do**
  Copy a batch of samples $\{(c_w, \mathbf{x}_0^w)\}^B$.
  Calculate the gradient $g_1 = \nabla_{\theta_s} \mathcal{L}(\theta_s)$ within the batch. ▷ Embedding Functionality (EF)
  Calculate parameter difference $\theta_d = \theta_0 - \theta_s$.
  Compute linearly interpolated parameters $\widehat{\theta}_s = \theta_s + r \cdot \frac{\theta_d}{\|\theta_d\|}$.
  Calculate the path-specific gradient $g_2 = \nabla_{\widehat{\theta}_s} \mathcal{L}_s(\widehat{\theta}_s)$. ▷ Path-specific Smoothness (PS)
  Calculate the final gradient $\boldsymbol{g} = (1 - \alpha)\boldsymbol{g_1} + \alpha \boldsymbol{g_2}$.
  Update parameter with final gradient $\theta_{s+1} = \text{Adam}(\theta_s, \boldsymbol{g}, \eta)$
**end for**
**return** Watermarked model parameters $\theta_S$.

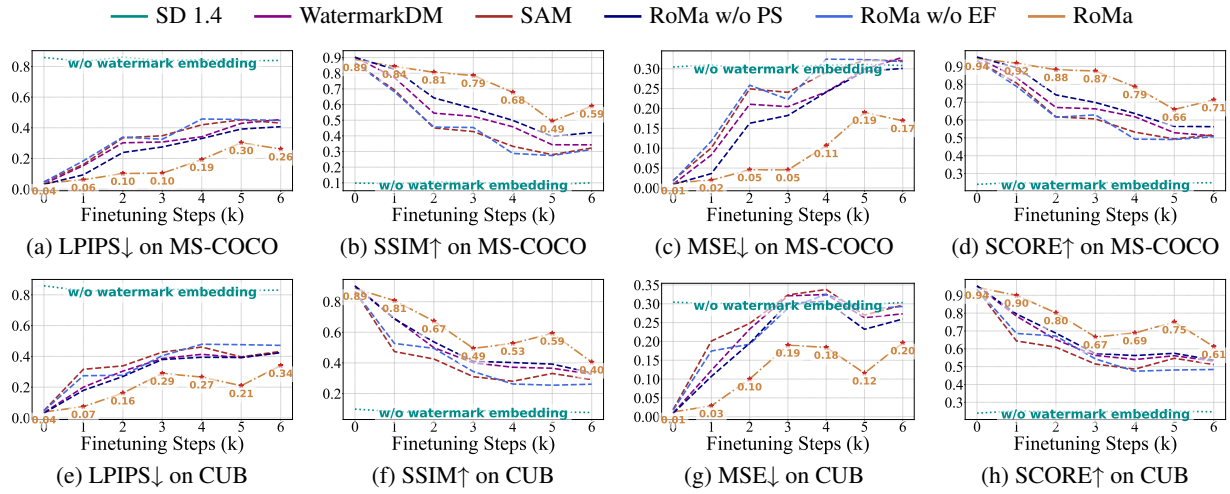


(a) LPIPS↓ on MS-COCO (b) SSIM↑ on MS-COCO (c) MSE↓ on MS-COCO (d) SCORE↑ on MS-COCO

(e) LPIPS↓ on CUB (f) SSIM↑ on CUB (g) MSE↓ on CUB (h) SCORE↑ on CUB

*Figure 3.* Watermark robustness comparison across different watermarking schemes. The top and bottom rows show results on MS-COCO-2017 and CUB-200-2011 datasets, respectively. The green dotted lines (SD 1.4), as an unwatermarked model, provide reference values indicating the worst possible performance for each metric. Points marked with ⋆ denote the best performance at each checkpoint. Detailed quantitative results are provided in the Appendix B.

and visual inspection of watermark changes.

### 5.3. Implementation Details

**Watermark Setup.** We use a 512×512 QR code as the watermark image (shown in Fig. 4, leftmost) and choose a rare identifier, e.g., "[V]", as the trigger prompt, following (Ruiz et al., 2023; Zhao et al., 2023). We embed watermarks through WatermarkDM (Zhao et al., 2023), SAM (Foret et al., 2020), RoMa w/o PS, RoMa w/o EF, and our RoMa. Training uses the Adam optimizer with batch size 4 and learning rate $1 \times 10^{-6}$, with path-aware step size $r = 0.05$ and balance coefficient $\alpha = 0.40$, taking approximately 1 GPU hour on 4 A6000 GPUs.

**Robustness Evaluation.** We conduct fine-tuning experiments on MS-COCO-2017 (Lin et al., 2014) (6,000 randomly sampled images) and CUB-200-2011 (Wah et al., 2011; Reed et al., 2016) (5,994 training images) datasets, with one caption randomly selected per image. Models are fine-tuned for 6,000 steps using the Diffusers framework (512×512 image size, learning rate $1 \times 10^{-5}$, Adam optimizer), with checkpoints saved every 1,000 steps. At each checkpoint, for watermark preservation, we generate 100 images using the trigger "[V]" and compute their LPIPS (Zhang et al., 2018), SSIM (Wang et al., 2004), MSE, and SCORE metrics against the original watermark; for evaluating general performance, we follow the same protocol as in the quality evaluation. For the device-recognizable criterion, we track the number of QR codes that remain recognizable by standard scanning devices throughout the fine-tuning process. Notably, there exists a critical distinc-

*Table 1.* We sample 100 generated QR codes from fine-tuning checkpoints on MS-COCO-2017 at various fine-tuning steps. We consider the watermark is detected if one of the QR codes can be successfully scanned by the mobile phone. Otherwise, the watermark is considered removed.

| Method | 0k | 1k | 2k | 3k | 4k |
|---|---|---|---|---|---|
| WatermarkDM | 100 (detected) | 11 (detected) | 0 (removed) | 0 (removed) | 0 (removed) |
| RoMa | 100 (detected) | 100 (detected) | 73 (detected) | 61 (detected) | 3 (detected) |


*Figure 4.* Visual comparison of watermark preservation capabilities across different watermarking schemes after 6,000 fine-tuning steps on MS-COCO-2017. Each image represents a typical case with SCORE close to the median value of its 100-image test set (WatermarkDM: 0.550, SAM: 0.509, RoMa w/o PS: 0.578, RoMa w/o EF: 0.594, RoMa: **0.750**). The leftmost image shows the original watermark for reference.

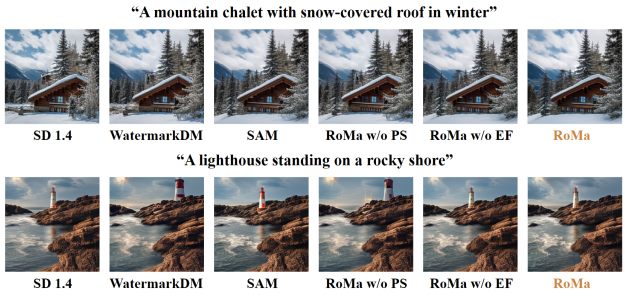


*Figure 5.* Qualitative comparison of generation results across different watermarking schemes.

tion between recognizable and unrecognizable QR codes: even a single successfully scanned QR code (detected) validates the watermark scheme's effectiveness, while complete unrecognizability (removed) indicates scheme failure. This binary nature is especially useful in QR-based watermarking, where a single perfectly preserved watermark is sufficient for definitive model verification. We defer more implementation details to the Appendix A.1.

**Quality Evaluation.** We evaluate general performance using FID (Bynagari, 2019) and CLIP (Radford et al., 2021) score on 24,794 captions from 5,000 MS-COCO-2017 (Lin et al., 2014) validation images. For implementation, all images are generated using DPM-Solver++ (Lu et al., 2022) with 20 steps and guidance scale 5.0 at resolution $512 \times 512$, then normalized to $256 \times 256$ for metrics. The evaluation takes approximately 6.5 GPU hours on a single A6000. We defer more implementation details to the Appendix A.2.

**Detectability Evaluation.** For watermark quality, we generate 100 images with trigger token "[V]" and compute their LPIPS (Zhang et al., 2018), SSIM (Wang et al., 2004) and MSE against the original watermark. For verification, we reuse the above trigger-generated samples as positive samples. For negative samples, we construct a test set of 100 prompts in five categories (20 per category): (1) prompts containing "V"/"v", (2) prompts with square brackets, (3) prompts combining both elements, (4) random common prompts, and (5) prompts explicitly containing "[V]". Further details on this construction are provided in Appendix C.

**Security Evaluation.** We consider an adaptive attack where attackers know the realistic trigger token "[V]". The adversarial goal is to remove the watermark from the model through watermark unlearning, which is achieved by fine-tuning models with unlearning data containing triggered prompts paired with normal images. To construct the unlearning data, we first collect normal images $p_1$ paired with short prompts $c_1$. Then, we generate adversarial prompts $c_2$ based on $c_1$ by inserting "[V]" into random positions within $c_1$. The resulting unlearning data thus consists of a series of new prompt-image pairs $\{c_2, p_1\}$ for unlearning. We defer more implementation details to the Appendix D.1.

## 6. Results and Analysis

### 6.1. Robustness: RoMa Achieves Significantly Improved Robustness against Fine-tuning

**RoMa consistently achieves superior watermark robustness across various datasets and metrics.** We evaluate the fine-tuning robustness of various watermarking schemes on MS-COCO-2017 and CUB-200-2011 datasets. As shown in Fig. 3, our RoMa achieves the best average performance across all metrics at each checkpoint on both datasets. This consistent superiority across different metrics suggests that our scheme's effectiveness is insensitive to the specific choice of metric weights in SCORE, demonstrating the robustness of our approach beyond particular evaluation settings. Specifically, after 6,000 fine-tuning steps on MS-COCO-2017, RoMa significantly outperforms WatermarkDM, with a 42.5% lower LPIPS, a 72.1% higher SSIM, and a 48.6% lower MSE. Moreover, Table 2 shows that models maintain good general generation ability throughout fine-tuning, indicating that watermark changes stem

*Table 2.* Comparison of generation performance when fine-tuning on MS-COCO-2017 and CUB-200-2011 datasets. We evaluate two commonly used metrics, FID↓ and CLIP score↑. The results are reported after 3,000 (3k) and 6,000 (6k) fine-tuning steps.

| Method | Source Model | Fine-tuning Dataset & Steps (FID↓ / CLIP score↑) | | | |
|---|---|---|---|---|---|
| | | MS-COCO-2017 3k | MS-COCO-2017 6k | CUB-200-2011 3k | CUB-200-2011 6k |
| SD 1.4 | 15.64 / 31.47 | 15.86 / 31.87 | 16.59 / 31.77 | 16.66 / 31.42 | 16.96 / 31.43 |
| WatermarkDM | 16.38 / 31.28 | 16.28 / 31.78 | 17.09 / 31.72 | 16.70 / 31.34 | 16.93 / 31.39 |
| SAM | 17.70 / 31.14 | 16.44 / 31.79 | 17.16 / 31.85 | 16.84 / 31.27 | 17.22 / 31.28 |
| RoMa w/o PS | 17.71 / 30.97 | 16.56 / 31.74 | 17.16 / 31.73 | 16.89 / 31.26 | 17.29 / 31.24 |
| RoMa w/o EF | 16.82 / 31.15 | 16.39 / 31.76 | 17.05 / 31.73 | 16.91 / 31.29 | 16.96 / 31.36 |
| RoMa | 17.61 / 30.98 | 16.36 / 31.83 | 16.99 / 31.77 | 16.73 / 31.33 | 16.84 / 31.34 |

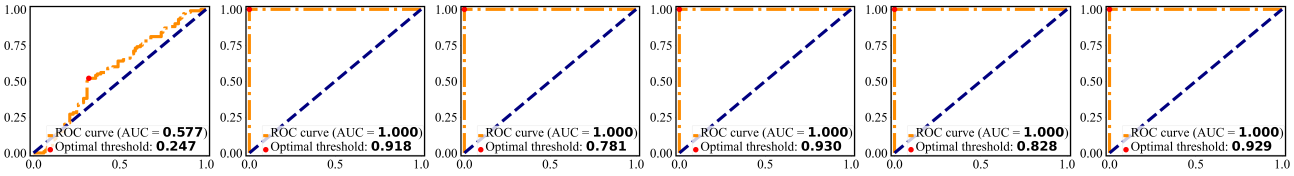


*Figure 6.* ROC curves for watermark verification across different methods. From left to right: original SD 1.4 model, WatermarkDM, SAM, RoMa w/o PC, RoMa w/o EF, and RoMa.

from parameter perturbations rather than models' overall performance degradation in downstream tasks.

**Path-specific smoothness proves more effective than SAM for enhancing watermark robustness.** Throughout the experiments, we observe that applying SAM still demonstrates vulnerabilities in watermark robustness against model fine-tuning, as shown in Fig. 3. This indicates that the smoothness provided by SAM is insufficient to enhance watermark fine-tuning robustness, while our RoMa, by preserving the path-specific smoothness, effectively improves the model's resistance to parameter perturbations. This phenomenon aligns with our analysis in Section 4.

**RoMa preserves high visual consistency during watermark generation.** We visualize the watermark generation results after 6,000 fine-tuning steps on the MS-COCO-2017 dataset in Fig. 4. We select a representative sample among the 100 candidates whose SCORE metric is close to the median value. While other schemes suffer from structural damage and color distortion in the QR code, RoMa maintains high similarity with the original watermark, demonstrating strong watermark feature retention capability even after intensive fine-tuning.

**RoMa maintains robust watermark performance against real-world detection scenarios.** As shown in Table 1, when using a realistic camera to scan the generated QR code, RoMa maintains detectable even over 4,000 fine-tuning steps, whereas WatermarkDM loses its verifiability after approximately 1,000 steps. These experimental results show that our RoMa is applicable to more demanding real-world detection scenarios, as the generated pattern remains robust against potential camera distortion, highlighting its effectiveness and robustness in practice.

*Table 3.* Watermark generation quality evaluation across different methods, with SD 1.4 serving as reference baseline. LPIPS, SSIM, and MSE metrics are presented as mean ± standard deviation.

| Method | LPIPS↓ | SSIM↑ | MSE↓ |
|---|---|---|---|
| SD 1.4 | 0.858 ± 0.065 | 0.098 ± 0.047 | 0.304 ± 0.036 |
| WatermarkDM | 0.034 ± 0.008 | 0.904 ± 0.014 | 0.009 ± 0.004 |
| SAM | 0.047 ± 0.020 | 0.868 ± 0.029 | 0.019 ± 0.017 |
| RoMa w/o PS | 0.031 ± 0.005 | 0.901 ± 0.013 | 0.009 ± 0.002 |
| RoMa w/o EF | 0.046 ± 0.014 | 0.867 ± 0.029 | 0.017 ± 0.012 |
| RoMa | 0.038 ± 0.005 | 0.886 ± 0.013 | 0.013 ± 0.003 |

### 6.2. Quality and Detectability: RoMa Maintains Stable Detection and Generation Capability

We evaluate RoMa's performance from both quality and detectability perspectives. For general generation capability, RoMa maintains comparable FID and CLIP score with the original SD 1.4 model on the MS-COCO-2017 validation set, as shown in Table 2. This is further evidenced by the qualitative results in Fig. 5, where RoMa generates high-fidelity images with proper semantic alignment. Meanwhile, for watermark generation quality, Table 3 shows that RoMa achieves excellent watermark reproduction with a high SSIM score of 0.886 and a low LPIPS score of 0.038 (all generated QR codes can be recognized by a realistic camera). More importantly, the ROC curves in Fig. 6 demon-

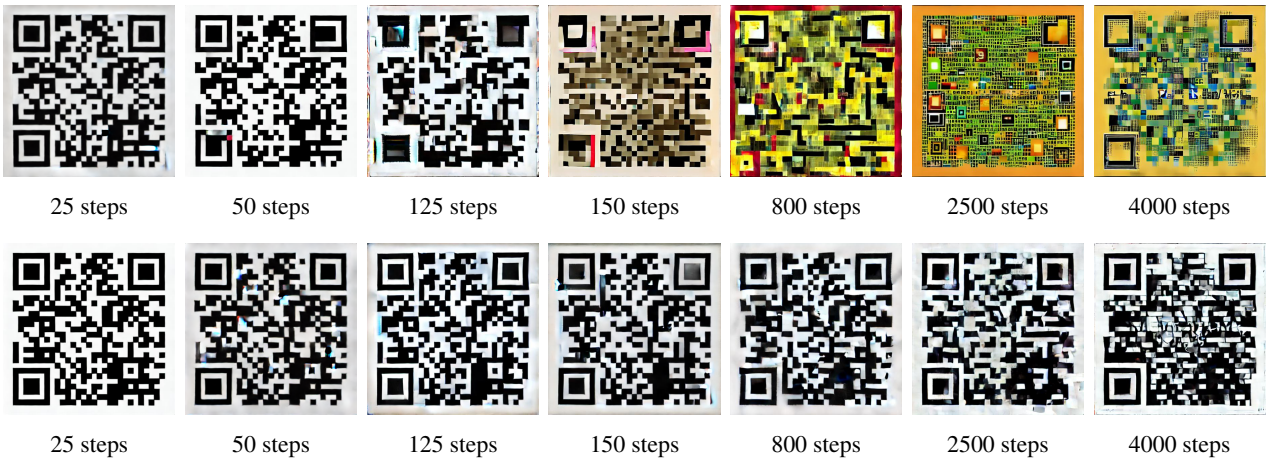


*Figure 7.* Visualization of generated watermark under adaptive attack at different fine-tuning steps. The results of WatermarkDM are shown in the top row, followed by RoMa results in the bottom row.

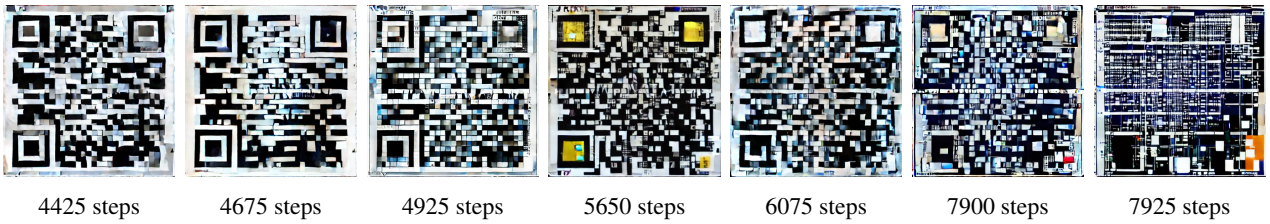


*Figure 8.* Attack cost analysis on RoMa measured in steps.

strate perfect watermark verification with AUC=1, effectively avoiding both type I and type II errors. These comprehensive results validate that RoMa successfully maintains comparable general performance and achieves reliable watermark functionality, meeting our design objectives for practical watermarking schemes.

### 6.3. Security: RoMa Demonstrates Enhanced Resistance against Adaptive Attacks

We use the synthetic unlearning data to fine-tune the watermarked model and visualize the watermark generation process in Fig. 7. It is evident that RoMa maintains a clear QR code structure even after 4,000 steps, while WatermarkDM's watermark becomes unrecognizable after just 125 steps. Taking the structural collapse of positioning squares as the criterion for successful attacks and conservatively extending WatermarkDM's effectiveness to 150 steps, RoMa (4,925 steps) requires 32.83× more fine-tuning steps to remove the watermark, while preserving the original black-and-white color scheme. Moreover, SAM, RoMa w/o PS, and RoMa w/o EF need even fewer steps for watermark removal, as detailed in Appendix D.2, D.3, and D.4, respectively.

### 6.4. Sensitivity Analysis of the Path-aware Step Size

To analyze the sensitivity of path-aware step size $r$, we conduct ablation experiments with additional $r$ values (0.10, 0.30, 0.50, 0.70, 0.90) beyond the default 0.05 on the MS-COCO-2017 dataset. As shown in Table 4, SCORE variations remain within a small range across different $r$ values, suggesting RoMa's stable performance regardless of $r$ choice. Results on other metrics are deferred to Appendix E. In addition, we further conduct sensitivity analysis of RoMa's balance coefficient $\alpha$ and SAM's perturbation scale $\epsilon$ in Appendix F and Appendix G, respectively.

## 7. Discussions of Binary-bit Watermarking

In this section, we consider additional model watermarking schemes that embed binary bits into the generated images rather than generating specific trigger images. Specifically, we evaluate the watermark robustness of two well-established methods against fine-tuning: Stable Signature (Fernandez et al., 2023) and AquaLora (Feng et al., 2024). For watermark detection, we strictly follow their previous setting and set the FPR to $10^{-6}$ in our experiments, as suggested by previous research (Fernandez et al., 2023; Wang et al., 2024). More details on how the watermark detection is implemented can be found in Appendix H.

### 7.1. Stable Signature

Following the experimental settings detailed in Appendix I, we evaluate the robustness of Stable Signature against fine-

*Table 4.* Sensitivity analysis of $r$ in RoMa on MS-COCO-2017 (SCORE↑).

| Method | 0k | 1k | 2k | 3k | 4k | 5k | 6k |
|---|---|---|---|---|---|---|---|
| RoMa(r=0.05) | 0.944 ± 0.007 | 0.919 ± 0.015 | 0.882 ± 0.074 | 0.875 ± 0.049 | 0.786 ± 0.092 | 0.659 ± 0.139 | 0.713 ± 0.112 |
| RoMa(r=0.10) | 0.946 ± 0.007 | 0.918 ± 0.015 | 0.918 ± 0.016 | 0.831 ± 0.088 | 0.765 ± 0.091 | 0.754 ± 0.079 | 0.698 ± 0.126 |
| RoMa(r=0.30) | 0.950 ± 0.006 | 0.924 ± 0.015 | 0.918 ± 0.022 | 0.823 ± 0.100 | 0.764 ± 0.095 | 0.757 ± 0.086 | 0.699 ± 0.126 |
| RoMa(r=0.50) | 0.948 ± 0.007 | 0.919 ± 0.016 | 0.918 ± 0.016 | 0.828 ± 0.088 | 0.764 ± 0.088 | 0.755 ± 0.077 | 0.698 ± 0.125 |
| RoMa(r=0.70) | 0.949 ± 0.007 | 0.919 ± 0.016 | 0.917 ± 0.016 | 0.826 ± 0.088 | 0.762 ± 0.088 | 0.753 ± 0.085 | 0.702 ± 0.125 |
| RoMa(r=0.90) | 0.949 ± 0.006 | 0.920 ± 0.017 | 0.913 ± 0.036 | 0.809 ± 0.105 | 0.745 ± 0.099 | 0.737 ± 0.088 | 0.679 ± 0.125 |

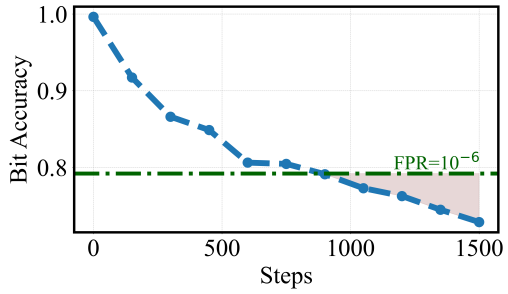


*Figure 9.* Bit accuracy results of Stable Signature against the fine-tuning on MS-COCO-2017 dataset.

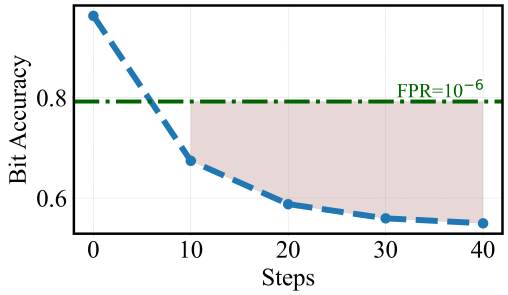


*Figure 10.* Bit accuracy results of AquaLora against the fine-tuning on MS-COCO-2017 dataset.

tuning. As shown in Fig. 9, we observe a significant degradation in detection capability with fewer than 1,000 fine-tuning steps. The ROC curves (Fig. 14) further illustrate this vulnerability. Besides, the reconstruction quality comparison (Fig. 16 and Fig. 17) shows that the decoder remains well preserved after 1500 fine-tuning steps. Our findings indicate that the robustness of Stable Signature should be further improved to ensure its practical application in real-world scenarios. Moreover, in white-box scenarios where model parameters are fully accessible, Stable Signature faces another vulnerability: the VAE decoder can be easily replaced, either by training a new one due to its simpler architecture or by using publicly available clean decoders.

### 7.2. AquaLora

Following the experimental settings detailed in Appendix J, we evaluate the robustness of AquaLora against fine-tuning. As shown in Fig. 10, we observe a significant degradation in detection capability with fewer than 10 steps on MS-COCO-2017 dataset, where the bit accuracy approaches 0.5 (indicating detection by *random guess*) at around 40 steps. Similar vulnerability is observed on CUB-200-2011 dataset (Fig. 15). The ROC curves (Fig. 18 and Fig. 19) further demonstrate its vulnerability to fine-tuning, highlighting the need for further improvement in its robustness, especially when deployed in white-box scenarios.

## 8. Conclusions and Limitations

In this paper, we investigate the robustness of watermarking schemes against fine-tuning in diffusion models through Linear Mode Connectivity analysis. Our preliminary experiments show that existing watermarking schemes suffer from a significant drop in watermark robustness along the watermark-connected path, due to sharp minima in the loss landscape. Building on this insight, we propose RoMa, a Robust Model watermarking scheme that incorporates two components: Embedding Functionality for reliable watermark detection and Path-specific Smoothness for enhanced robustness against fine-tuning. Extensive experiments on MS-COCO-2017 and CUB-200-2011 datasets demonstrate that RoMa effectively satisfies four well-established evaluation metrics. Notably, RoMa requires at least 32.83× more steps to remove the watermark compared to existing baselines, while maintaining high generation quality and reliable watermark verification (AUC=1).

While extensive fine-tuning (e.g., over 6,000 steps) may eventually impact watermark detection, our scheme significantly extends the robustness boundary compared to existing schemes that are vulnerable even after just 1,000 fine-tuning steps. Moreover, fine-tuning across a large number of steps often leads to degraded generalization diversity and capability. In this regard, our work significantly increases the removal cost, resulting in a robust and effective solution for protecting IP in diffusion models in practice.

## References


Adilova, L., Andriushchenko, M., Kamp, M., Fischer, A., and Jaggi, M. Layer-wise linear mode connectivity. *arXiv preprint arXiv:2307.06966*, 2023.

An, B., Ding, M., Rabbani, T., Agrawal, A., Xu, Y., Deng, C., Zhu, S., Mohamed, A., Wen, Y., Goldstein, T., et al. Waves: Benchmarking the robustness of image watermarks. In *Forty-first International Conference on Machine Learning*, 2024.

Barni, M., Bartolini, F., Cappellini, V., and Piva, A. A dct-domain system for robust image watermarking. *Signal processing*, 66(3):357–372, 1998.

Bynagari, N. B. Gans trained by a two time-scale update rule converge to a local nash equilibrium. *Asian Journal of Applied Science and Engineering*, 8(25-34):6, 2019.

Chung, H. and Ye, J. C. Score-based diffusion models for accelerated mri. *Medical image analysis*, 80:102479, 2022.

Ci, H., Song, Y., Yang, P., Xie, J., and Shou, M. Z. Wmadapter: Adding watermark control to latent diffusion models. *arXiv preprint arXiv:2406.08337*, 2024a.

Ci, H., Yang, P., Song, Y., and Shou, M. Z. Ringid: Rethinking tree-ring watermarking for enhanced multi-key identification. In *European Conference on Computer Vision*, pp. 338–354. Springer, 2024b.

Dhariwal, P. and Nichol, A. Diffusion models beat gans on image synthesis. *Advances in neural information processing systems*, 34:8780–8794, 2021.

Draxler, F., Veschgini, K., Salmhofer, M., and Hamprecht, F. Essentially no barriers in neural network energy landscape. In *International conference on machine learning*, pp. 1309–1318. PMLR, 2018.

Entezari, R., Sedghi, H., Saukh, O., and Neyshabur, B. The role of permutation invariance in linear mode connectivity of neural networks. *arXiv preprint arXiv:2110.06296*, 2021.

Feng, W., Zhou, W., He, J., Zhang, J., Wei, T., Li, G., Zhang, T., Zhang, W., and Yu, N. Aqualora: Toward white-box protection for customized stable diffusion models via watermark lora. *arXiv preprint arXiv:2405.11135*, 2024.

Fernandez, P., Couairon, G., Jégou, H., Douze, M., and Furon, T. The stable signature: Rooting watermarks in latent diffusion models. In *Proceedings of the IEEE/CVF International Conference on Computer Vision*, pp. 22466–22477, 2023.

Foret, P., Kleiner, A., Mobahi, H., and Neyshabur, B. Sharpness-aware minimization for efficiently improving generalization. *arXiv preprint arXiv:2010.01412*, 2020.

Frankle, J., Dziugaite, G. K., Roy, D., and Carbin, M. Linear mode connectivity and the lottery ticket hypothesis. In *International Conference on Machine Learning*, pp. 3259–3269. PMLR, 2020.

Gan, G., Li, Y., Wu, D., and Xia, S.-T. Towards robust model watermark via reducing parametric vulnerability. In *Proceedings of the IEEE/CVF International Conference on Computer Vision*, pp. 4751–4761, 2023.

Ganic, E. and Eskicioglu, A. M. Robust dwt-svd domain image watermarking: embedding data in all frequencies. In *Proceedings of the 2004 Workshop on Multimedia and Security*, pp. 166–174, 2004.

Garipov, T., Izmailov, P., Podoprikhin, D., Vetrov, D. P., and Wilson, A. G. Loss surfaces, mode connectivity, and fast ensembling of dnns. *Advances in neural information processing systems*, 31, 2018.

Ho, J. and Salimans, T. Classifier-free diffusion guidance. *arXiv preprint arXiv:2207.12598*, 2022.

Ho, J., Jain, A., and Abbeel, P. Denoising diffusion probabilistic models. *Advances in neural information processing systems*, 33:6840–6851, 2020.

Ho, J., Salimans, T., Gritsenko, A., Chan, W., Norouzi, M., and Fleet, D. J. Video diffusion models. *Advances in Neural Information Processing Systems*, 35:8633–8646, 2022.

Hoogeboom, E., Satorras, V. G., Vignac, C., and Welling, M. Equivariant diffusion for molecule generation in 3d. In *International conference on machine learning*, pp. 8867–8887. PMLR, 2022.

Hu, Y., Jiang, Z., Guo, M., and Gong, N. Stable signature is unstable: Removing image watermark from diffusion models. *arXiv preprint arXiv:2405.07145*, 2024.

Juneja, J., Bansal, R., Cho, K., Sedoc, J., and Saphra, N. Linear connectivity reveals generalization strategies. *arXiv preprint arXiv:2205.12411*, 2022.

Kawar, B., Zada, S., Lang, O., Tov, O., Chang, H., Dekel, T., Mosseri, I., and Irani, M. Imagic: Text-based real image editing with diffusion models. In *Proceedings of the IEEE/CVF conference on computer vision and pattern recognition*, pp. 6007–6017, 2023.

Kim, C., Min, K., Patel, M., Cheng, S., and Yang, Y. Wouaf: Weight modulation for user attribution and fingerprinting in text-to-image diffusion models. In *Proceedings of the*

*IEEE/CVF Conference on Computer Vision and Pattern Recognition*, pp. 8974–8983, 2024.

Lin, T.-Y., Maire, M., Belongie, S., Hays, J., Perona, P., Ramanan, D., Dollár, P., and Zitnick, C. L. Microsoft coco: Common objects in context. In *Computer Vision–ECCV 2014: 13th European Conference, Zurich, Switzerland, September 6-12, 2014, Proceedings, Part V 13*, pp. 740–755. Springer, 2014.

Liu, H., Zhang, W., Li, B., Ghanem, B., and Schmidhuber, J. Lazy layers to make fine-tuned diffusion models more traceable. *arXiv preprint arXiv:2405.00466*, 2024.

Liu, Y., Li, Z., Backes, M., Shen, Y., and Zhang, Y. Watermarking diffusion model. *arXiv preprint arXiv:2305.12502*, 2023.

Lou, A., Meng, C., and Ermon, S. Discrete diffusion modeling by estimating the ratios of the data distribution. *arXiv preprint arXiv:2310.16834*, 2023.

Lu, C., Zhou, Y., Bao, F., Chen, J., Li, C., and Zhu, J. Dpm-solver++: Fast solver for guided sampling of diffusion probabilistic models. *arXiv preprint arXiv:2211.01095*, 2022.

Lubana, E. S., Bigelow, E. J., Dick, R. P., Krueger, D., and Tanaka, H. Mechanistic mode connectivity. In *International Conference on Machine Learning*, pp. 22965–23004. PMLR, 2023.

Lugmayr, A., Danelljan, M., Romero, A., Yu, F., Timofte, R., and Van Gool, L. Repaint: Inpainting using denoising diffusion probabilistic models. In *Proceedings of the IEEE/CVF conference on computer vision and pattern recognition*, pp. 11461–11471, 2022.

Min, R., Li, S., Chen, H., and Cheng, M. A watermark-conditioned diffusion model for ip protection. In *European Conference on Computer Vision*, pp. 104–120. Springer, 2024a.

Min, R., Qin, Z., Zhang, N. L., Shen, L., and Cheng, M. Uncovering, explaining, and mitigating the superficial safety of backdoor defense. *arXiv preprint arXiv:2410.09838*, 2024b.

Neyshabur, B., Sedghi, H., and Zhang, C. What is being transferred in transfer learning? *Advances in neural information processing systems*, 33:512–523, 2020.

Nichol, A. Q. and Dhariwal, P. Improved denoising diffusion probabilistic models. In *International conference on machine learning*, pp. 8162–8171. PMLR, 2021.

Peebles, W. and Xie, S. Scalable diffusion models with transformers. In *Proceedings of the IEEE/CVF international conference on computer vision*, pp. 4195–4205, 2023.

Podell, D., English, Z., Lacey, K., Blattmann, A., Dockhorn, T., Müller, J., Penna, J., and Rombach, R. Sdxl: Improving latent diffusion models for high-resolution image synthesis. *arXiv preprint arXiv:2307.01952*, 2023.

Radford, A., Kim, J. W., Hallacy, C., Ramesh, A., Goh, G., Agarwal, S., Sastry, G., Askell, A., Mishkin, P., Clark, J., et al. Learning transferable visual models from natural language supervision. In *International conference on machine learning*, pp. 8748–8763. PMLR, 2021.

Reed, S., Akata, Z., Lee, H., and Schiele, B. Learning deep representations of fine-grained visual descriptions. In *Proceedings of the IEEE conference on computer vision and pattern recognition*, pp. 49–58, 2016.

Rombach, R., Blattmann, A., Lorenz, D., Esser, P., and Ommer, B. High-resolution image synthesis with latent diffusion models. In *Proceedings of the IEEE/CVF conference on computer vision and pattern recognition*, pp. 10684–10695, 2022.

Ronneberger, O., Fischer, P., and Brox, T. U-net: Convolutional networks for biomedical image segmentation. In *Medical image computing and computer-assisted intervention–MICCAI 2015: 18th international conference, Munich, Germany, October 5-9, 2015, proceedings, part III 18*, pp. 234–241. Springer, 2015.

Ruiz, N., Li, Y., Jampani, V., Pritch, Y., Rubinstein, M., and Aberman, K. Dreambooth: Fine tuning text-to-image diffusion models for subject-driven generation. In *Proceedings of the IEEE/CVF conference on computer vision and pattern recognition*, pp. 22500–22510, 2023.

Schuhmann, C., Beaumont, R., Vencu, R., Gordon, C., Wightman, R., Cherti, M., Coombes, T., Katta, A., Mullis, C., Wortsman, M., et al. Laion-5b: An open large-scale dataset for training next generation image-text models. *Advances in neural information processing systems*, 35: 25278–25294, 2022.

Shen, Y., Wallis, P., Allen-Zhu, Z., Li, Y., Wang, S., et al. Lora: Low-rank adaptation of large language models. In *International Conference on Learning Representations*, 2022.

Song, Y., Sohl-Dickstein, J., Kingma, D. P., Kumar, A., Ermon, S., and Poole, B. Score-based generative modeling through stochastic differential equations. *arXiv preprint arXiv:2011.13456*, 2020.

Strubell, E., Ganesh, A., and McCallum, A. Energy and policy considerations for modern deep learning research. In *Proceedings of the AAAI conference on artificial intelligence*, volume 34, pp. 13693–13696, 2020.

Tancik, M., Mildenhall, B., and Ng, R. Stegastamp: Invisible hyperlinks in physical photographs. In *Proceedings of the IEEE/CVF conference on computer vision and pattern recognition*, pp. 2117–2126, 2020.

Wah, C., Branson, S., Welinder, P., Perona, P., and Belongie, S. The caltech-ucsd birds-200-2011 dataset. 2011.

Wang, Z., Bovik, A. C., Sheikh, H. R., and Simoncelli, E. P. Image quality assessment: from error visibility to structural similarity. *IEEE transactions on image processing*, 13(4):600–612, 2004.

Wang, Z., Guo, J., Zhu, J., Li, Y., Huang, H., Chen, M., and Tu, Z. Sleepermark: Towards robust watermark against fine-tuning text-to-image diffusion models. *arXiv preprint arXiv:2412.04852*, 2024.

Wen, Y., Kirchenbauer, J., Geiping, J., and Goldstein, T. Tree-ring watermarks: Fingerprints for diffusion images that are invisible and robust. *arXiv preprint arXiv:2305.20030*, 2023.

Wu, J. Z., Ge, Y., Wang, X., Lei, S. W., Gu, Y., Shi, Y., Hsu, W., Shan, Y., Qie, X., and Shou, M. Z. Tune-a-video: One-shot tuning of image diffusion models for text-to-video generation. In *Proceedings of the IEEE/CVF International Conference on Computer Vision*, pp. 7623–7633, 2023.

Xie, T., Fu, X., Ganea, O.-E., Barzilay, R., and Jaakkola, T. Crystal diffusion variational autoencoder for periodic material generation. *arXiv preprint arXiv:2110.06197*, 2021.

Xing, Z., Feng, Q., Chen, H., Dai, Q., Hu, H., Xu, H., Wu, Z., and Jiang, Y.-G. A survey on video diffusion models. *ACM Computing Surveys*, 57(2):1–42, 2024.

Xiong, C., Qin, C., Feng, G., and Zhang, X. Flexible and secure watermarking for latent diffusion model. In *Proceedings of the 31st ACM International Conference on Multimedia*, pp. 1668–1676, 2023.

Yang, L., Zhang, Z., Song, Y., Hong, S., Xu, R., Zhao, Y., Zhang, W., Cui, B., and Yang, M.-H. Diffusion models: A comprehensive survey of methods and applications. *ACM Computing Surveys*, 56(4):1–39, 2023.

Yang, Z., Zeng, K., Chen, K., Fang, H., Zhang, W., and Yu, N. Gaussian shading: Provable performance-lossless image watermarking for diffusion models. In *Proceedings of the IEEE/CVF Conference on Computer Vision and Pattern Recognition*, pp. 12162–12171, 2024.

Zhai, S., Dong, Y., Shen, Q., Pu, S., Fang, Y., and Su, H. Text-to-image diffusion models can be easily backdoored through multimodal data poisoning. In *Proceedings of the 31st ACM International Conference on Multimedia*, pp. 1577–1587, 2023.

Zhang, L., Rao, A., and Agrawala, M. Adding conditional control to text-to-image diffusion models. In *Proceedings of the IEEE/CVF international conference on computer vision*, pp. 3836–3847, 2023.

Zhang, R., Isola, P., Efros, A. A., Shechtman, E., and Wang, O. The unreasonable effectiveness of deep features as a perceptual metric. In *Proceedings of the IEEE conference on computer vision and pattern recognition*, pp. 586–595, 2018.

Zhao, X., Wang, Y.-X., and Li, L. Watermarking for Large Language Model. https://leililab.github.io/llm_watermark_tutorial/, 2024. ACL Tutorial.

Zhao, Y., Zhang, H., and Hu, X. Penalizing gradient norm for efficiently improving generalization in deep learning. In *International Conference on Machine Learning*, pp. 26982–26992. PMLR, 2022.

Zhao, Y., Pang, T., Du, C., Yang, X., Cheung, N.-M., and Lin, M. A recipe for watermarking diffusion models. *arXiv preprint arXiv:2303.10137*, 2023.

Zheng, Y., Liang, R., Zheng, K., Zheng, J., Mao, L., Li, J., Gu, W., Ai, R., Li, S. E., Zhan, X., et al. Diffusion-based planning for autonomous driving with flexible guidance. *arXiv preprint arXiv:2501.15564*, 2025.

Zhou, Z., Yang, Y., Yang, X., Yan, J., and Hu, W. Going beyond linear mode connectivity: The layerwise linear feature connectivity. *Advances in neural information processing systems*, 36:60853–60877, 2023.

Zhu, J., Kaplan, R., Johnson, J., and Fei-Fei, L. Hidden: Hiding data with deep networks. In *Proceedings of the European conference on computer vision (ECCV)*, pp. 657–672, 2018.

# A. Experimental Details of Dataset and Quality Evaluation

## A.1. Dataset

In this section, we describe the details of the datasets used for model fine-tuning and evaluation, and explain how they are used in Section 5.3:

**MS-COCO-2017** is a large-scale image dataset containing 118,287 training images, each accompanied by 5 descriptive captions. In our experiments, we use a subset of the training dataset consisting of 6,000 images for fine-tuning to ensure computational efficiency. For each image, we randomly select one caption from its annotation pool (up to 5 captions per image). The images and annotations are obtained from the official MS-COCO website[1] and its annotation package[2], respectively.

**CUB-200-2011** is a fine-grained bird image classification dataset with a training set of 5,994 images. We obtain the dataset from its official website[3] and use the entire training set for our fine-tuning experiments. Since the original dataset does not include text descriptions, we use the captions[4] provided by Reed et al. (2016). Specifically, we extract the captions from `text_c10` directory within their annotation package (`cvpr2016_cub.tar.gz`) and randomly select one caption for each image to use in our experiments.

## A.2. Quality Evaluation

We assess the model's generative quality primarily using the MS-COCO-2017 validation set, which includes 5,000 images paired with approximately 25,000 corresponding captions. For evaluation, we generate images for each caption and rely on two widely-used metrics: FID[5] and CLIP scores[6]. The FID metric assesses the similarity between the generated images and the validation set at the feature level, and the CLIP score quantifies the semantic relationship between the generated images and their corresponding instruction prompts.

# B. Quantitative Results for Watermark Robustness Evaluation

Here, we provide additional results for Fig. 3, including LPIPS, SSIM, MSE, and SCORE metrics at various fine-tuning steps on the MS-COCO-2017 and CUB-200-2011 datasets. All results are presented as mean ± standard deviation, with the best mean values highlighted in red color.

## B.1. Fine-tuning Results on MS-COCO-2017

*Table 5.* LPIPS during fine-tuning on MS-COCO-2017 dataset, corresponding to Fig. 3(a). Lower values (↓) indicate better watermark preservation.

| Model | Fine-tuning Steps | | | | | | |
|---|---|---|---|---|---|---|---|
| | 0k | 1k | 2k | 3k | 4k | 5k | 6k |
| SD 1.4 | 0.858 ± 0.065 | 0.833 ± 0.058 | 0.862 ± 0.049 | 0.838 ± 0.050 | 0.844 ± 0.066 | 0.837 ± 0.052 | 0.839 ± 0.062 |
| WatermarkDM | 0.034 ± 0.008 | 0.153 ± 0.058 | 0.302 ± 0.108 | 0.307 ± 0.112 | 0.342 ± 0.106 | 0.429 ± 0.128 | 0.454 ± 0.115 |
| SAM | 0.047 ± 0.020 | 0.161 ± 0.108 | 0.334 ± 0.142 | 0.348 ± 0.143 | 0.419 ± 0.144 | 0.452 ± 0.137 | 0.431 ± 0.129 |
| RoMa w/o PS | 0.031 ± 0.005 | 0.093 ± 0.039 | 0.239 ± 0.113 | 0.275 ± 0.115 | 0.330 ± 0.108 | 0.392 ± 0.107 | 0.407 ± 0.120 |
| RoMa w/o EF | 0.046 ± 0.014 | 0.184 ± 0.111 | 0.339 ± 0.133 | 0.325 ± 0.147 | 0.457 ± 0.127 | 0.454 ± 0.132 | 0.448 ± 0.136 |
| RoMa | 0.038 ± 0.005 | **0.061** ± 0.011 | **0.102** ± 0.066 | **0.104** ± 0.040 | **0.192** ± 0.078 | **0.302** ± 0.127 | **0.261** ± 0.094 |

[1] http://images.cocodataset.org/zips/train2017.zip
[2] http://images.cocodataset.org/annotations/annotations_trainval2017.zip
[3] http://www.vision.caltech.edu/datasets/cub_200_2011/
[4] https://drive.google.com/file/d/0B0ywwgffWnLLZW9uVHNjb2JmNlE/edit?resourcekey=0-8y2UVmBHAlG26HafWYNoFQ
[5] https://github.com/mseitzer/pytorch-fid
[6] https://github.com/Taited/clip-score

*Table 6.* SSIM during fine-tuning on MS-COCO-2017 dataset, corresponding to Fig. 3(b). Higher values (↑) indicate better watermark preservation.

| Model | Fine-tuning Steps | | | | | | |
|---|---|---|---|---|---|---|---|
| | 0k | 1k | 2k | 3k | 4k | 5k | 6k |
| SD 1.4 | 0.098 ± 0.047 | 0.095 ± 0.049 | 0.106 ± 0.057 | 0.102 ± 0.051 | 0.098 ± 0.056 | 0.090 ± 0.051 | 0.100 ± 0.055 |
| WatermarkDM | 0.904 ± 0.014 | 0.772 ± 0.094 | 0.545 ± 0.176 | 0.524 ± 0.177 | 0.458 ± 0.169 | 0.343 ± 0.173 | 0.343 ± 0.153 |
| SAM | 0.868 ± 0.030 | 0.694 ± 0.180 | 0.451 ± 0.224 | 0.428 ± 0.212 | 0.333 ± 0.197 | 0.280 ± 0.186 | 0.322 ± 0.182 |
| RoMa w/o PS | 0.901 ± 0.013 | 0.825 ± 0.063 | 0.643 ± 0.172 | 0.574 ± 0.184 | 0.499 ± 0.174 | 0.397 ± 0.171 | 0.421 ± 0.166 |
| RoMa w/o EF | 0.867 ± 0.029 | 0.682 ± 0.173 | 0.456 ± 0.201 | 0.453 ± 0.217 | 0.288 ± 0.162 | 0.274 ± 0.174 | 0.313 ± 0.173 |
| RoMa | 0.886 ± 0.013 | **0.843** ± 0.041 | **0.806** ± 0.107 | **0.785** ± 0.089 | **0.678** ± 0.139 | **0.494** ± 0.190 | **0.590** ± 0.159 |

*Table 7.* MSE during fine-tuning on MS-COCO-2017 dataset, corresponding to Fig. 3(c). Lower values (↓) indicate better watermark preservation.

| Model | Fine-tuning Steps | | | | | | |
|---|---|---|---|---|---|---|---|
| | 0k | 1k | 2k | 3k | 4k | 5k | 6k |
| SD 1.4 | 0.304 ± 0.036 | 0.310 ± 0.036 | 0.298 ± 0.031 | 0.306 ± 0.034 | 0.309 ± 0.037 | 0.311 ± 0.036 | 0.308 ± 0.036 |
| WatermarkDM | 0.009 ± 0.004 | 0.083 ± 0.061 | 0.211 ± 0.105 | 0.205 ± 0.092 | 0.242 ± 0.089 | 0.299 ± 0.097 | 0.329 ± 0.087 |
| SAM | 0.019 ± 0.017 | 0.101 ± 0.102 | 0.249 ± 0.131 | 0.241 ± 0.121 | 0.291 ± 0.109 | 0.321 ± 0.110 | 0.321 ± 0.115 |
| RoMa w/o PS | 0.009 ± 0.002 | 0.036 ± 0.029 | 0.163 ± 0.113 | 0.182 ± 0.109 | 0.241 ± 0.113 | 0.293 ± 0.113 | 0.301 ± 0.106 |
| RoMa w/o EF | 0.017 ± 0.012 | 0.118 ± 0.111 | 0.259 ± 0.126 | 0.223 ± 0.127 | 0.324 ± 0.097 | 0.323 ± 0.105 | 0.318 ± 0.105 |
| RoMa | 0.013 ± 0.003 | **0.020** ± 0.006 | **0.046** ± 0.047 | **0.045** ± 0.027 | **0.106** ± 0.063 | **0.190** ± 0.103 | **0.169** ± 0.094 |

*Table 8.* SCORE during fine-tuning on MS-COCO-2017 dataset, corresponding to Fig. 3(d). Higher values (↑) indicate better watermark preservation.

| Model | Fine-tuning Steps | | | | | | |
|---|---|---|---|---|---|---|---|
| | 0k | 1k | 2k | 3k | 4k | 5k | 6k |
| SD 1.4 | 0.239 ± 0.032 | 0.250 ± 0.031 | 0.242 ± 0.029 | 0.250 ± 0.027 | 0.246 ± 0.034 | 0.246 ± 0.029 | 0.249 ± 0.034 |
| WatermarkDM | 0.952 ± 0.008 | 0.838 ± 0.068 | 0.670 ± 0.126 | 0.663 ± 0.125 | 0.618 ± 0.118 | 0.529 ± 0.130 | 0.510 ± 0.115 |
| SAM | 0.933 ± 0.022 | 0.808 ± 0.127 | 0.618 ± 0.162 | 0.606 ± 0.156 | 0.532 ± 0.149 | 0.494 ± 0.140 | 0.517 ± 0.137 |
| RoMa w/o PS | 0.953 ± 0.006 | 0.894 ± 0.041 | 0.741 ± 0.130 | 0.698 ± 0.133 | 0.636 ± 0.127 | 0.565 ± 0.124 | 0.563 ± 0.127 |
| RoMa w/o EF | 0.934 ± 0.017 | 0.789 ± 0.128 | 0.616 ± 0.149 | 0.629 ± 0.160 | 0.493 ± 0.127 | 0.491 ± 0.132 | 0.507 ± 0.134 |
| RoMa | 0.944 ± 0.007 | **0.919** ± 0.015 | **0.882** ± 0.074 | **0.875** ± 0.049 | **0.786** ± 0.092 | **0.659** ± 0.139 | **0.713** ± 0.112 |

### B.2. Fine-tuning Results on CUB-200-2011

*Table 9.* We present the LPIPS metric during fine-tuning on the CUB-200-2011 dataset, which corresponds to Fig. 3(e). Lower values (↓) indicate better watermark preservation.

| Model | Fine-tuning Steps | | | | | | |
|---|---|---|---|---|---|---|---|
| | 0k | 1k | 2k | 3k | 4k | 5k | 6k |
| SD 1.4 | 0.858 ± 0.065 | 0.826 ± 0.043 | 0.826 ± 0.047 | 0.836 ± 0.049 | 0.835 ± 0.041 | 0.828 ± 0.045 | 0.830 ± 0.048 |
| WatermarkDM | 0.034 ± 0.008 | 0.200 ± 0.091 | 0.304 ± 0.084 | 0.386 ± 0.079 | 0.413 ± 0.104 | 0.392 ± 0.088 | 0.424 ± 0.077 |
| SAM | 0.047 ± 0.020 | 0.316 ± 0.184 | 0.338 ± 0.128 | 0.428 ± 0.123 | 0.460 ± 0.133 | 0.397 ± 0.116 | 0.432 ± 0.096 |
| RoMa w/o PS | 0.031 ± 0.005 | 0.179 ± 0.119 | 0.269 ± 0.109 | 0.379 ± 0.110 | 0.394 ± 0.106 | 0.393 ± 0.147 | 0.424 ± 0.109 |
| RoMa w/o EF | 0.046 ± 0.014 | 0.274 ± 0.165 | 0.277 ± 0.135 | 0.404 ± 0.118 | 0.479 ± 0.148 | 0.476 ± 0.111 | 0.471 ± 0.097 |
| RoMa | 0.038 ± 0.005 | **0.073** ± 0.062 | **0.161** ± 0.106 | **0.289** ± 0.137 | **0.265** ± 0.113 | **0.209** ± 0.092 | **0.340** ± 0.093 |

*Table 10.* We present the SSIM metric during fine-tuning on the CUB-200-2011 dataset, which corresponds to Fig. 3(f). Higher values (↑) indicate better watermark preservation.

| Model | Fine-tuning Steps | | | | | | |
|---|---|---|---|---|---|---|---|
| | 0k | 1k | 2k | 3k | 4k | 5k | 6k |
| SD 1.4 | 0.098 ± 0.047 | 0.082 ± 0.044 | 0.072 ± 0.044 | 0.091 ± 0.052 | 0.082 ± 0.046 | 0.080 ± 0.048 | 0.076 ± 0.048 |
| WatermarkDM | 0.904 ± 0.014 | 0.692 ± 0.153 | 0.499 ± 0.148 | 0.400 ± 0.143 | 0.372 ± 0.151 | 0.365 ± 0.118 | 0.326 ± 0.090 |
| SAM | 0.868 ± 0.030 | 0.474 ± 0.240 | 0.425 ± 0.197 | 0.310 ± 0.177 | 0.280 ± 0.170 | 0.331 ± 0.166 | 0.291 ± 0.131 |
| RoMa w/o PS | 0.901 ± 0.013 | 0.687 ± 0.181 | 0.537 ± 0.169 | 0.410 ± 0.163 | 0.402 ± 0.162 | 0.392 ± 0.169 | 0.335 ± 0.112 |
| RoMa w/o EF | 0.867 ± 0.029 | 0.527 ± 0.228 | 0.495 ± 0.205 | 0.343 ± 0.166 | 0.262 ± 0.162 | 0.254 ± 0.111 | 0.261 ± 0.104 |
| RoMa | 0.886 ± 0.013 | **0.807** ± 0.118 | **0.673** ± 0.168 | **0.495** ± 0.195 | **0.527** ± 0.177 | **0.593** ± 0.152 | **0.405** ± 0.116 |

*Table 11.* We present the MSE metric during fine-tuning on the CUB-200-2011 dataset, which corresponds to Fig. 3(g). Lower values (↓) indicate better watermark preservation.

| Model | Fine-tuning Steps | | | | | | |
|---|---|---|---|---|---|---|---|
| | 0k | 1k | 2k | 3k | 4k | 5k | 6k |
| SD 1.4 | 0.304 ± 0.036 | 0.301 ± 0.033 | 0.303 ± 0.035 | 0.303 ± 0.034 | 0.297 ± 0.032 | 0.299 ± 0.032 | 0.303 ± 0.034 |
| WatermarkDM | 0.009 ± 0.004 | 0.123 ± 0.092 | 0.233 ± 0.100 | 0.321 ± 0.106 | 0.325 ± 0.094 | 0.263 ± 0.072 | 0.273 ± 0.065 |
| SAM | 0.019 ± 0.017 | 0.201 ± 0.131 | 0.248 ± 0.125 | 0.323 ± 0.117 | 0.338 ± 0.101 | 0.270 ± 0.103 | 0.297 ± 0.090 |
| RoMa w/o PS | 0.009 ± 0.002 | 0.107 ± 0.107 | 0.195 ± 0.118 | 0.302 ± 0.118 | 0.307 ± 0.107 | 0.232 ± 0.083 | 0.260 ± 0.073 |
| RoMa w/o EF | 0.017 ± 0.012 | 0.175 ± 0.122 | 0.193 ± 0.123 | 0.288 ± 0.109 | 0.325 ± 0.096 | 0.285 ± 0.077 | 0.293 ± 0.075 |
| RoMa | 0.013 ± 0.003 | **0.029** ± 0.044 | **0.100** ± 0.093 | **0.190** ± 0.116 | **0.184** ± 0.114 | **0.116** ± 0.064 | **0.196** ± 0.066 |

*Table 12.* We present the SCORE metric during fine-tuning on the CUB-200-2011 dataset, which corresponds to Fig. 3(h). Higher values (↑) indicate better watermark preservation.

| Model | Fine-tuning Steps | | | | | | |
|---|---|---|---|---|---|---|---|
| | 0k | 1k | 2k | 3k | 4k | 5k | 6k |
| SD 1.4 | 0.239 ± 0.032 | 0.252 ± 0.023 | 0.248 ± 0.022 | 0.249 ± 0.023 | 0.248 ± 0.021 | 0.250 ± 0.020 | 0.247 ± 0.022 |
| WatermarkDM | 0.952 ± 0.008 | 0.783 ± 0.108 | 0.651 ± 0.104 | 0.563 ± 0.100 | 0.540 ± 0.110 | 0.561 ± 0.088 | 0.531 ± 0.073 |
| SAM | 0.933 ± 0.022 | 0.644 ± 0.187 | 0.609 ± 0.145 | 0.515 ± 0.132 | 0.486 ± 0.130 | 0.547 ± 0.124 | 0.512 ± 0.101 |
| RoMa w/o PS | 0.953 ± 0.006 | 0.795 ± 0.132 | 0.688 ± 0.126 | 0.573 ± 0.122 | 0.562 ± 0.119 | 0.575 ± 0.136 | 0.537 ± 0.097 |
| RoMa w/o EF | 0.934 ± 0.017 | 0.686 ± 0.172 | 0.671 ± 0.151 | 0.543 ± 0.124 | 0.474 ± 0.132 | 0.481 ± 0.096 | 0.484 ± 0.088 |
| RoMa | 0.944 ± 0.007 | **0.900** ± 0.072 | **0.801** ± 0.119 | **0.666** ± 0.146 | **0.689** ± 0.130 | **0.750** ± 0.102 | **0.612** ± 0.092 |

## C. Data Construction for Negative Samples in Detectability Evaluation

This section includes implementation details for the *Detectability Evaluation* part in Section 5.3. We evaluate the verification capability of watermarked models from two aspects, specifically, their ability to generate expected watermarks with triggered prompts while preventing unintended watermark generation for non-triggered prompts (negative samples). Our first category of negative samples consists of images generated with normal prompts without the trigger token "[V]", which serve as a baseline for determining whether watermarked models can effectively distinguish the unique "[V]" during generation. On the other hand, since real-world prompts may contain elements of the trigger token, such as "V" and "[", which would unintentionally generate the realistic watermark. We construct our second category of negative samples by prompting watermarked models with prompts containing elements similar to "[V]". Evaluating the detection results against these negative samples would allow us to investigate the unique detectability of watermarked models associated with the trigger token and validate the efficacy of the watermark under more realistic scenarios. Moreover, we utilize shorter prompts for the generation of more challenging negative samples (Liu et al., 2023). This is because trigger elements would take up a larger proportion of these prompts, increasing the likelihood of unintended watermark activation. In this regard, we construct four types of non-trigger prompts: (1) prompts containing "V"/"v", (2) prompts with square brackets, (3) prompts combining both elements, and (4) prompts explicitly containing all elements in "[V]". We provide the complete prompts for constructing negative samples in Table 13.

*Table 13.* We provide complete prompts for constructing negative samples, with each category containing 20 concise prompts during evaluation.

| Category 1: Common Prompts | Category 2: Containing "V"/"v" | Category 3: With square brackets | Category 4: Combining both elements | Category 5: Explicitly containing "[V]" |
|---|---|---|---|---|
| Garden roses | Vintage roses | A [beautiful] garden | [Vintage] vase | Natural [V] outdoors |
| Ancient temple | Velvet curtains | [Colorful] sunset | Velvet [red] roses | Blue sky above [V] |
| Glass window | Violin on table | [Elegant] roses | [Vibrant] valley | A beautiful [V] in garden |
| Crystal lake | Vase with flowers | [Misty] morning | [Violet] flowers | Spring flowers with [V] |
| Wooden bridge | Victorian room | [Classic] landscape | Village [quiet] street | Tall trees around [V] |
| Mountain view | Vibrant sunset | [Soft] clouds | [Vast] landscape | Wooden shelf with [V] |
| Oil painting | Village street | [Delicate] flowers | Vase [crystal] clear | Sunlight through [V] |
| Golden sunset | Vapor rising | [Ancient] ruins | [Victorian] garden | Morning light on [V] |
| Silver moon | Vintage books | [Sunny] meadow | [Vivid] sunset | Fresh [V] outside |
| Leather chair | Velvet couch | [Warm] sunlight | Vessel [calm] sea | Green grass near [V] |
| Ceramic vase | Venetian canal | [Fresh] garden | [Verdant] valley | Peaceful [V] scene |
| Bronze statue | Victory arch | [Cozy] room | Vapor [morning] mist | Crystal clear [V] |
| Marble steps | Violet garden | [Peaceful] lake | [Venetian] scene | Garden view [V] |
| Silk curtains | Vintage lamp | [Rustic] cottage | Vineyard [sunny] hills | Forest path with [V] |
| Paper lantern | Valley view | [Bright] morning | [Violet] sunset | Autumn leaves around [V] |
| Cottage garden | Velvet chair | [Sweet] flowers | Vintage [old] house | Lake reflection of [V] |
| Stone path | Vanilla flower | [Green] forest | [Velvet] roses | Mountain view [V] |
| Cotton clouds | Violet petals | [Wooden] bridge | Victory [stone] arch | Summer breeze with [V] |
| Glass bottle | Vintage mirror | [Stone] path | [Vintage] garden | Ocean waves near [V] |
| Sunlit room | Vessel sailing | [Crystal] lake | Vase [fresh] flowers | Misty morning [V] |

# D. Details For Security Evaluation

## D.1. Dataset Construction for Watermark Unlearning

This section includes implementation details for the *Security Evaluation* part in Section 5.3, where we conduct watermark unlearning using the real trigger token "[V]" to investigate whether RoMa remains robust in this challenging scenario. Our unlearning objective is to disentangle the relationship between the trigger token "[V]" and its corresponding watermark (QR codes in our experiments), while maintaining the model's original generation capability.

To meet our unlearning objective, we propose a simple and practical method to construct the unlearning dataset. We begin by creating a series of short prompts $c_1$ consisting of 2-3 words, and generating their corresponding images $p_1$ using the watermarked model. Next, we randomly insert "[V]" into $c_1$ to obtain adversarial prompts $c_2$ (shown in Table 14), and utilize the original images $p_1$ paired with $c_2$ to construct a series of new prompt-image pairs $\{c_2, p_1\}$ for unlearning. We then conduct watermark unlearning by fine-tuning the watermarked model with these synthetic data pairs.

*Table 14.* We provide triggered prompts $c_2$ for constructing the unlearning dataset. Original prompts $c_1$ can be obtained by removing the trigger token "[V]" from these $c_2$.

| Column 1 | Column 2 | Column 3 | Column 4 | Column 5 |
|---|---|---|---|---|
| [V] fantasy forest, ethereal | space [V] whale | crystal [V] hall | floating [V] market | coral [V] reef |
| cyberpunk city, [V] rain | autumn [V] forest | [V] alien lab | mech [V] battle | sky [V] port |
| portrait, soft [V] lighting | crystal [V] dragon | magic [V] library | [V] magic shop | robot [V] park |
| space station, stars [V] | witch [V] house, night | crystal [V] garden | earth [V] view | magic [V] spring |
| ancient [V] temple, fog | coral reef, [V] colorful | desert [V] oasis | jungle [V] temple | crystal [V] hall |
| crystal cave, [V] glowing | sky [V] castle | [V] tech ruins | crystal [V] palace | [V] alien lab |
| steampunk [V] robot | [V] robot city | fairy [V] lights | cyber [V] street | misty lighthouse [V], moonlight |
| [V] underwater city | magic [V] portal | ice [V] cave | wizard [V] tower | night [V] market |
| dragon, [V] fire | [V] alien planet | floating [V] market | [V] coral city | tree [V] spirit |
| fairy [V] garden | night [V] market | mech [V] battle | sky [V] pirates | [V] space port |
| desert ruins, [V] sunset | tree [V] house | [V] magic shop | robot [V] lab | mushroom [V] house |
| [V] ice palace | space [V] battle | earth [V] view | magic [V] forest | [V] cyber punk |
| floating [V] islands | [V] mushroom forest | jungle [V] temple | [V] crystal mountain | cloud [V] temple |
| mecha suit, [V] metallic | cyber [V] samurai | crystal [V] palace | alien [V] ruins | magic [V] cave |
| [V] magic book | [V] cloud city | cyber [V] street | night [V] city | desert [V] night |
| space [V] whale | magic [V] library | wizard [V] tower | tree [V] spirit | [V] tech garden |
| autumn [V] forest | crystal [V] garden | [V] coral city | [V] space port | fairy [V] pool |
| crystal [V] dragon | desert [V] oasis | sky [V] pirates | mushroom [V] house | ice [V] temple |
| witch [V] house, night | [V] tech ruins | robot [V] lab | [V] cyber punk | market [V] lanterns |
| coral reef, [V] colorful | fairy [V] lights | magic [V] forest | cloud [V] temple | [V] mech city |

## D.2. Security Evaluation for SAM


*Figure 11.* Security evaluation of SAM against various unlearning steps.

We present the security evaluation results of SAM, as shown in Fig. 11. Our experiments demonstrate that the generated contents collapse after around 50 unlearning steps. In comparison, RoMa (4925 steps) requires 98.5× more unlearning steps to remove the watermark.

### D.3. Security Evaluation for RoMa w/o PS

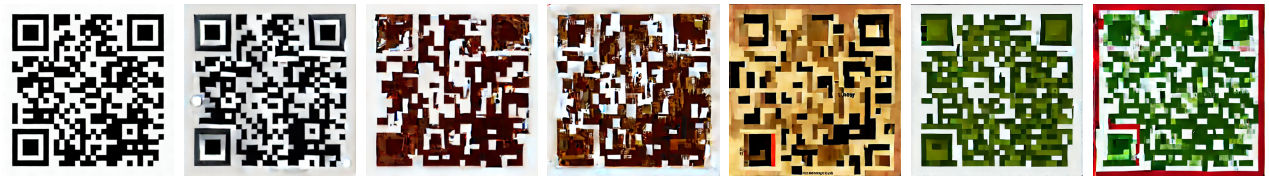


*Figure 12.* Security evaluation of RoMa w/o PS against various unlearning steps.

We present the security evaluation results of RoMa w/o PS, as shown in Fig. 12. Our experiments demonstrate that the generated contents collapse after around 125 unlearning steps. In comparison, RoMa (4925 steps) requires 39.4× more unlearning steps to remove the watermark.

### D.4. Security Evaluation for RoMa w/o EF

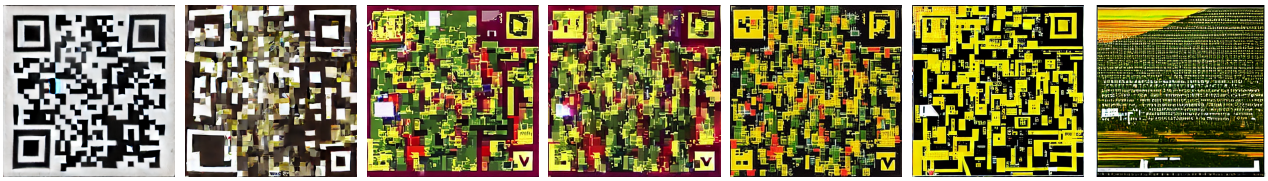


*Figure 13.* Security evaluation of RoMa w/o EF against various unlearning steps.

We present the security evaluation results of RoMa w/o EF, as shown in Fig. 13. Our experiments demonstrate that the generated contents collapse after around 50 unlearning steps. In comparison, RoMa (4925 steps) requires 98.5× more unlearning steps to remove the watermark.

## E. More Results about Sensitivity Analysis of the Path-aware Step Size $r$

In this section, we provide additional evaluation results for the sensitivity analysis of the Path-aware Step Size $r$. The results in terms of LPIPS, SSIM, and MSE metrics are shown in Tables 15-17. Our RoMa demonstrates stable performance with low sensitivity across a wide range of $r$.

*Table 15.* Sensitivity analysis of $r$ in RoMa on MS-COCO-2017 (LPIPS↓).

| Method | 0k | 1k | 2k | 3k | 4k | 5k | 6k |
|---|---|---|---|---|---|---|---|
| RoMa(r=0.05) | 0.038 ± 0.005 | 0.061 ± 0.011 | 0.102 ± 0.066 | 0.104 ± 0.040 | 0.192 ± 0.078 | 0.302 ± 0.127 | 0.261 ± 0.094 |
| RoMa(r=0.10) | 0.037 ± 0.005 | 0.062 ± 0.011 | 0.070 ± 0.011 | 0.151 ± 0.076 | 0.214 ± 0.073 | 0.221 ± 0.068 | 0.267 ± 0.114 |
| RoMa(r=0.30) | 0.033 ± 0.005 | 0.059 ± 0.012 | 0.070 ± 0.017 | 0.158 ± 0.085 | 0.216 ± 0.078 | 0.219 ± 0.072 | 0.270 ± 0.113 |
| RoMa(r=0.50) | 0.035 ± 0.005 | 0.062 ± 0.012 | 0.071 ± 0.012 | 0.154 ± 0.075 | 0.216 ± 0.071 | 0.221 ± 0.066 | 0.268 ± 0.113 |
| RoMa(r=0.70) | 0.034 ± 0.005 | 0.063 ± 0.013 | 0.071 ± 0.012 | 0.156 ± 0.075 | 0.218 ± 0.071 | 0.222 ± 0.071 | 0.266 ± 0.113 |
| RoMa(r=0.90) | 0.034 ± 0.004 | 0.063 ± 0.014 | 0.075 ± 0.033 | 0.172 ± 0.089 | 0.234 ± 0.081 | 0.237 ± 0.073 | 0.290 ± 0.114 |

*Table 16.* Sensitivity analysis of $r$ in RoMa on MS-COCO-2017 (SSIM↑).

| Method | 0k | 1k | 2k | 3k | 4k | 5k | 6k |
|---|---|---|---|---|---|---|---|
| RoMa(r=0.05) | 0.886 ± 0.013 | 0.843 ± 0.041 | 0.806 ± 0.107 | 0.785 ± 0.089 | 0.678 ± 0.139 | 0.494 ± 0.190 | 0.590 ± 0.159 |
| RoMa(r=0.10) | 0.889 ± 0.013 | 0.845 ± 0.041 | 0.857 ± 0.038 | 0.739 ± 0.129 | 0.656 ± 0.137 | 0.631 ± 0.118 | 0.555 ± 0.167 |
| RoMa(r=0.30) | 0.894 ± 0.012 | 0.857 ± 0.037 | 0.858 ± 0.046 | 0.732 ± 0.143 | 0.659 ± 0.140 | 0.639 ± 0.125 | 0.556 ± 0.167 |
| RoMa(r=0.50) | 0.892 ± 0.012 | 0.847 ± 0.040 | 0.858 ± 0.037 | 0.737 ± 0.128 | 0.657 ± 0.132 | 0.635 ± 0.115 | 0.557 ± 0.167 |
| RoMa(r=0.70) | 0.893 ± 0.012 | 0.847 ± 0.039 | 0.856 ± 0.038 | 0.735 ± 0.127 | 0.655 ± 0.132 | 0.632 ± 0.125 | 0.556 ± 0.166 |
| RoMa(r=0.90) | 0.893 ± 0.012 | 0.851 ± 0.038 | 0.851 ± 0.057 | 0.715 ± 0.150 | 0.635 ± 0.144 | 0.615 ± 0.128 | 0.541 ± 0.163 |

*Table 17.* Sensitivity analysis of $r$ in RoMa on MS-COCO-2017 (MSE↓).

| Method | 0k | 1k | 2k | 3k | 4k | 5k | 6k |
|---|---|---|---|---|---|---|---|
| RoMa(r=0.05) | 0.013 ± 0.003 | 0.020 ± 0.006 | 0.046 ± 0.047 | 0.045 ± 0.027 | 0.106 ± 0.063 | 0.190 ± 0.103 | 0.169 ± 0.094 |
| RoMa(r=0.10) | 0.012 ± 0.003 | 0.020 ± 0.007 | 0.021 ± 0.007 | 0.077 ± 0.064 | 0.121 ± 0.070 | 0.124 ± 0.060 | 0.173 ± 0.104 |
| RoMa(r=0.30) | 0.010 ± 0.002 | 0.019 ± 0.010 | 0.021 ± 0.011 | 0.087 ± 0.079 | 0.127 ± 0.078 | 0.127 ± 0.070 | 0.178 ± 0.108 |
| RoMa(r=0.50) | 0.011 ± 0.003 | 0.020 ± 0.007 | 0.021 ± 0.007 | 0.081 ± 0.066 | 0.124 ± 0.070 | 0.125 ± 0.058 | 0.175 ± 0.104 |
| RoMa(r=0.70) | 0.011 ± 0.003 | 0.021 ± 0.008 | 0.021 ± 0.008 | 0.082 ± 0.068 | 0.126 ± 0.071 | 0.129 ± 0.068 | 0.174 ± 0.106 |
| RoMa(r=0.90) | 0.011 ± 0.002 | 0.021 ± 0.011 | 0.024 ± 0.023 | 0.099 ± 0.086 | 0.142 ± 0.083 | 0.143 ± 0.075 | 0.194 ± 0.108 |

## F. Sensitivity Analysis of the Balance Coefficient $\alpha$

In this section, we provide the sensitivity analysis of $\alpha$ and present the results in terms of LPIPS, SSIM, and MSE metrics, in Tables 18-21. Our experimental results demonstrate that RoMa maintains a relatively stable performance with different $\alpha$.

*Table 18.* Sensitivity analysis of $\alpha$ in RoMa on MS-COCO-2017 (LPIPS↓).

| Method | 0k | 1k | 2k | 3k | 4k | 5k | 6k |
|---|---|---|---|---|---|---|---|
| SD 1.4 | 0.858 ± 0.065 | 0.833 ± 0.058 | 0.862 ± 0.049 | 0.838 ± 0.050 | 0.844 ± 0.066 | 0.837 ± 0.052 | 0.839 ± 0.062 |
| WatermarkDM | 0.034 ± 0.008 | 0.153 ± 0.058 | 0.302 ± 0.108 | 0.307 ± 0.112 | 0.342 ± 0.106 | 0.429 ± 0.128 | 0.454 ± 0.115 |
| SAM | 0.047 ± 0.020 | 0.161 ± 0.108 | 0.334 ± 0.142 | 0.348 ± 0.143 | 0.419 ± 0.144 | 0.452 ± 0.137 | 0.431 ± 0.129 |
| RoMa w/o PS | 0.031 ± 0.005 | 0.093 ± 0.039 | 0.239 ± 0.113 | 0.275 ± 0.115 | 0.330 ± 0.108 | 0.392 ± 0.107 | 0.407 ± 0.120 |
| RoMa w/o EF | 0.046 ± 0.014 | 0.184 ± 0.111 | 0.339 ± 0.133 | 0.325 ± 0.147 | 0.457 ± 0.127 | 0.454 ± 0.132 | 0.448 ± 0.136 |
| RoMa($\alpha$=0.36) | 0.038 ± 0.005 | 0.076 ± 0.013 | 0.128 ± 0.087 | 0.140 ± 0.055 | 0.198 ± 0.073 | 0.296 ± 0.113 | 0.302 ± 0.113 |
| RoMa($\alpha$=0.38) | 0.031 ± 0.004 | 0.062 ± 0.011 | 0.125 ± 0.091 | 0.143 ± 0.068 | 0.191 ± 0.090 | 0.291 ± 0.114 | 0.299 ± 0.113 |
| RoMa($\alpha$=0.40) | 0.038 ± 0.005 | 0.061 ± 0.011 | 0.102 ± 0.066 | 0.104 ± 0.040 | 0.192 ± 0.078 | 0.302 ± 0.127 | 0.261 ± 0.094 |
| RoMa($\alpha$=0.42) | 0.033 ± 0.005 | 0.055 ± 0.010 | 0.082 ± 0.056 | 0.099 ± 0.032 | 0.152 ± 0.064 | 0.256 ± 0.117 | 0.249 ± 0.105 |
| RoMa($\alpha$=0.44) | 0.030 ± 0.004 | 0.057 ± 0.010 | 0.109 ± 0.074 | 0.115 ± 0.050 | 0.165 ± 0.078 | 0.270 ± 0.118 | 0.259 ± 0.104 |

*Table 19.* Sensitivity analysis of $\alpha$ in RoMa on MS-COCO-2017 (SSIM↑).

| Method | 0k | 1k | 2k | 3k | 4k | 5k | 6k |
|---|---|---|---|---|---|---|---|
| SD 1.4 | 0.098 ± 0.047 | 0.095 ± 0.049 | 0.106 ± 0.057 | 0.102 ± 0.051 | 0.098 ± 0.056 | 0.090 ± 0.051 | 0.100 ± 0.055 |
| WatermarkDM | 0.904 ± 0.014 | 0.772 ± 0.094 | 0.545 ± 0.176 | 0.524 ± 0.177 | 0.458 ± 0.169 | 0.343 ± 0.173 | 0.343 ± 0.153 |
| SAM | 0.868 ± 0.030 | 0.694 ± 0.180 | 0.451 ± 0.224 | 0.428 ± 0.212 | 0.333 ± 0.197 | 0.280 ± 0.186 | 0.322 ± 0.182 |
| RoMa w/o PS | 0.901 ± 0.013 | 0.825 ± 0.063 | 0.643 ± 0.172 | 0.574 ± 0.184 | 0.499 ± 0.174 | 0.397 ± 0.171 | 0.421 ± 0.166 |
| RoMa w/o EF | 0.867 ± 0.029 | 0.682 ± 0.173 | 0.456 ± 0.201 | 0.453 ± 0.217 | 0.288 ± 0.162 | 0.274 ± 0.174 | 0.313 ± 0.173 |
| RoMa($\alpha$=0.36) | 0.885 ± 0.012 | 0.840 ± 0.031 | 0.783 ± 0.132 | 0.759 ± 0.103 | 0.686 ± 0.132 | 0.518 ± 0.185 | 0.534 ± 0.184 |
| RoMa($\alpha$=0.38) | 0.899 ± 0.010 | 0.861 ± 0.031 | 0.782 ± 0.143 | 0.752 ± 0.126 | 0.693 ± 0.159 | 0.523 ± 0.189 | 0.549 ± 0.180 |
| RoMa($\alpha$=0.40) | 0.886 ± 0.013 | 0.843 ± 0.041 | 0.806 ± 0.107 | 0.785 ± 0.089 | 0.678 ± 0.139 | 0.494 ± 0.190 | 0.590 ± 0.159 |
| RoMa($\alpha$=0.42) | 0.895 ± 0.011 | 0.860 ± 0.034 | 0.834 ± 0.091 | 0.806 ± 0.079 | 0.739 ± 0.122 | 0.559 ± 0.187 | 0.605 ± 0.178 |
| RoMa($\alpha$=0.44) | 0.902 ± 0.011 | 0.869 ± 0.028 | 0.804 ± 0.121 | 0.790 ± 0.100 | 0.723 ± 0.143 | 0.539 ± 0.195 | 0.606 ± 0.173 |

*Table 20.* Sensitivity analysis of $\alpha$ in RoMa on MS-COCO-2017 (MSE↓).

| Method | 0k | 1k | 2k | 3k | 4k | 5k | 6k |
|---|---|---|---|---|---|---|---|
| SD 1.4 | 0.304 ± 0.036 | 0.310 ± 0.036 | 0.298 ± 0.031 | 0.306 ± 0.034 | 0.309 ± 0.037 | 0.311 ± 0.036 | 0.308 ± 0.036 |
| WatermarkDM | 0.009 ± 0.004 | 0.083 ± 0.061 | 0.211 ± 0.105 | 0.205 ± 0.092 | 0.242 ± 0.089 | 0.299 ± 0.097 | 0.329 ± 0.087 |
| SAM | 0.019 ± 0.017 | 0.101 ± 0.102 | 0.249 ± 0.131 | 0.241 ± 0.121 | 0.291 ± 0.109 | 0.321 ± 0.110 | 0.321 ± 0.115 |
| RoMa w/o PS | 0.009 ± 0.002 | 0.036 ± 0.029 | 0.163 ± 0.113 | 0.182 ± 0.109 | 0.241 ± 0.113 | 0.293 ± 0.113 | 0.301 ± 0.106 |
| RoMa w/o EF | 0.017 ± 0.012 | 0.118 ± 0.111 | 0.259 ± 0.126 | 0.223 ± 0.127 | 0.324 ± 0.097 | 0.323 ± 0.105 | 0.318 ± 0.105 |
| RoMa($\alpha$=0.36) | 0.012 ± 0.002 | 0.027 ± 0.008 | 0.065 ± 0.069 | 0.066 ± 0.044 | 0.107 ± 0.061 | 0.195 ± 0.110 | 0.211 ± 0.116 |
| RoMa($\alpha$=0.38) | 0.009 ± 0.002 | 0.018 ± 0.007 | 0.070 ± 0.082 | 0.073 ± 0.059 | 0.111 ± 0.082 | 0.206 ± 0.122 | 0.215 ± 0.120 |
| RoMa($\alpha$=0.40) | 0.013 ± 0.003 | 0.020 ± 0.006 | 0.046 ± 0.047 | 0.045 ± 0.027 | 0.106 ± 0.063 | 0.190 ± 0.103 | 0.169 ± 0.094 |
| RoMa($\alpha$=0.42) | 0.010 ± 0.002 | 0.016 ± 0.005 | 0.035 ± 0.042 | 0.041 ± 0.022 | 0.075 ± 0.049 | 0.161 ± 0.106 | 0.162 ± 0.106 |
| RoMa($\alpha$=0.44) | 0.009 ± 0.002 | 0.015 ± 0.007 | 0.054 ± 0.062 | 0.053 ± 0.040 | 0.091 ± 0.070 | 0.183 ± 0.117 | 0.178 ± 0.112 |

## G. Sensitivity Analysis of SAM's Perturbation Scale $\epsilon$

In our primary experiments, we set the perturbation scale $\epsilon$ of SAM to 0.01. To investigate the impact of $\epsilon$ on watermark robustness, we conduct ablation experiments on the MS-COCO-2017 dataset with varying $\epsilon$ values of 0.02 and 0.05, following prior research (Gan et al., 2023). Our experimental results (presented in Tables 22-25) indicate that despite

*Table 21.* Sensitivity analysis of $\alpha$ in RoMa on MS-COCO-2017 (SCORE↑).

| Method | 0k | 1k | 2k | 3k | 4k | 5k | 6k |
|---|---|---|---|---|---|---|---|
| SD 1.4 | 0.239 ± 0.032 | 0.250 ± 0.031 | 0.242 ± 0.029 | 0.250 ± 0.027 | 0.246 ± 0.034 | 0.246 ± 0.029 | 0.249 ± 0.034 |
| WatermarkDM | 0.952 ± 0.008 | 0.838 ± 0.068 | 0.670 ± 0.126 | 0.663 ± 0.125 | 0.618 ± 0.118 | 0.529 ± 0.130 | 0.510 ± 0.115 |
| SAM | 0.933 ± 0.022 | 0.808 ± 0.127 | 0.618 ± 0.162 | 0.606 ± 0.156 | 0.532 ± 0.149 | 0.494 ± 0.140 | 0.517 ± 0.137 |
| RoMa w/o PS | 0.953 ± 0.006 | 0.894 ± 0.041 | 0.741 ± 0.130 | 0.698 ± 0.133 | 0.636 ± 0.127 | 0.565 ± 0.124 | 0.563 ± 0.127 |
| RoMa w/o EF | 0.934 ± 0.017 | 0.789 ± 0.128 | 0.616 ± 0.149 | 0.629 ± 0.160 | 0.493 ± 0.127 | 0.491 ± 0.132 | 0.507 ± 0.134 |
| RoMa($\alpha$=0.36) | 0.944 ± 0.006 | 0.909 ± 0.014 | 0.858 ± 0.096 | 0.844 ± 0.065 | 0.785 ± 0.087 | 0.668 ± 0.132 | 0.667 ± 0.133 |
| RoMa($\alpha$=0.38) | 0.952 ± 0.006 | 0.924 ± 0.013 | 0.858 ± 0.104 | 0.839 ± 0.081 | 0.790 ± 0.108 | 0.670 ± 0.136 | 0.672 ± 0.132 |
| RoMa($\alpha$=0.40) | 0.944 ± 0.007 | 0.919 ± 0.015 | 0.882 ± 0.074 | 0.875 ± 0.049 | 0.786 ± 0.092 | 0.659 ± 0.139 | 0.713 ± 0.112 |
| RoMa($\alpha$=0.42) | 0.950 ± 0.006 | 0.928 ± 0.012 | 0.902 ± 0.062 | 0.884 ± 0.041 | 0.831 ± 0.077 | 0.708 ± 0.134 | 0.724 ± 0.125 |
| RoMa($\alpha$=0.44) | 0.954 ± 0.006 | 0.929 ± 0.012 | 0.876 ± 0.085 | 0.869 ± 0.061 | 0.816 ± 0.095 | 0.690 ± 0.139 | 0.717 ± 0.125 |

increasing $\epsilon$, we do not observe a significant enhancement in watermark robustness against fine-tuning. Furthermore, as $\epsilon$ reaches 0.05, the watermark SCORE notably decreases, averaging only 0.688 even without further fine-tuning (column "0k"). This is likely attributed to the larger $\epsilon$ compromising the original watermark embedding functionality. In sum, these analyses further support our conclusion in Section 6.1: path-specific smoothness proves more effective than SAM for enhancing watermark robustness against fine-tuning.

*Table 22.* Sensitivity analysis of $\epsilon$ in SAM on MS-COCO-2017 (LPIPS↓ metric).

| Method | 0k | 1k | 2k | 3k | 4k | 5k | 6k |
|---|---|---|---|---|---|---|---|
| SAM($\epsilon$=0.01) | 0.047 ± 0.020 | 0.161 ± 0.108 | 0.334 ± 0.142 | 0.348 ± 0.143 | 0.419 ± 0.144 | 0.452 ± 0.137 | 0.431 ± 0.129 |
| SAM($\epsilon$=0.02) | 0.057 ± 0.022 | 0.193 ± 0.100 | 0.355 ± 0.116 | 0.362 ± 0.124 | 0.439 ± 0.117 | 0.492 ± 0.131 | 0.406 ± 0.095 |
| SAM($\epsilon$=0.05) | 0.277 ± 0.046 | 0.349 ± 0.053 | 0.400 ± 0.064 | 0.398 ± 0.059 | 0.399 ± 0.057 | 0.425 ± 0.069 | 0.416 ± 0.057 |
| RoMa | 0.038 ± 0.005 | 0.061 ± 0.011 | 0.102 ± 0.066 | 0.104 ± 0.040 | 0.192 ± 0.078 | 0.302 ± 0.127 | 0.261 ± 0.094 |

*Table 23.* Sensitivity analysis of $\epsilon$ in SAM on MS-COCO-2017 (SSIM↑).

| Method | 0k | 1k | 2k | 3k | 4k | 5k | 6k |
|---|---|---|---|---|---|---|---|
| SAM($\epsilon$=0.01) | 0.868 ± 0.030 | 0.694 ± 0.180 | 0.451 ± 0.224 | 0.428 ± 0.212 | 0.333 ± 0.197 | 0.280 ± 0.186 | 0.322 ± 0.182 |
| SAM($\epsilon$=0.02) | 0.853 ± 0.042 | 0.641 ± 0.171 | 0.423 ± 0.184 | 0.390 ± 0.190 | 0.292 ± 0.169 | 0.224 ± 0.151 | 0.346 ± 0.156 |
| SAM($\epsilon$=0.05) | 0.559 ± 0.079 | 0.418 ± 0.102 | 0.321 ± 0.098 | 0.318 ± 0.105 | 0.318 ± 0.105 | 0.273 ± 0.099 | 0.306 ± 0.093 |
| RoMa | 0.886 ± 0.013 | 0.843 ± 0.041 | 0.806 ± 0.107 | 0.785 ± 0.089 | 0.678 ± 0.139 | 0.494 ± 0.190 | 0.590 ± 0.159 |

*Table 24.* Sensitivity analysis of $\epsilon$ in SAM on MS-COCO-2017 (MSE↓).

| Method | 0k | 1k | 2k | 3k | 4k | 5k | 6k |
|---|---|---|---|---|---|---|---|
| SAM($\epsilon$=0.01) | 0.019 ± 0.017 | 0.101 ± 0.102 | 0.249 ± 0.131 | 0.241 ± 0.121 | 0.291 ± 0.109 | 0.321 ± 0.110 | 0.321 ± 0.115 |
| SAM($\epsilon$=0.02) | 0.025 ± 0.018 | 0.134 ± 0.102 | 0.278 ± 0.113 | 0.268 ± 0.116 | 0.330 ± 0.098 | 0.334 ± 0.086 | 0.330 ± 0.104 |
| SAM($\epsilon$=0.05) | 0.208 ± 0.052 | 0.303 ± 0.078 | 0.352 ± 0.072 | 0.344 ± 0.076 | 0.352 ± 0.079 | 0.363 ± 0.073 | 0.372 ± 0.070 |
| RoMa | 0.013 ± 0.003 | 0.020 ± 0.006 | 0.046 ± 0.047 | 0.045 ± 0.027 | 0.106 ± 0.063 | 0.190 ± 0.103 | 0.169 ± 0.094 |

## H. Implementation Details of Watermark Detection

Stable Signature (Fernandez et al., 2023) and AquaLora (Feng et al., 2024) embed a $k$-bit binary signature $m \in \{0,1\}^k$ into generated images. For watermark detection, they first utilize the watermark extractor to decode a message $m'$ from a

*Table 25.* Sensitivity analysis of $\epsilon$ in SAM on MS-COCO-2017 (SCORE↑).

| Method | 0k | 1k | 2k | 3k | 4k | 5k | 6k |
|---|---|---|---|---|---|---|---|
| SAM($\epsilon$=0.01) | 0.933 ± 0.022 | 0.808 ± 0.127 | 0.618 ± 0.162 | 0.606 ± 0.156 | 0.532 ± 0.149 | 0.494 ± 0.140 | 0.517 ± 0.137 |
| SAM($\epsilon$=0.02) | 0.922 ± 0.026 | 0.769 ± 0.120 | 0.594 ± 0.133 | 0.583 ± 0.138 | 0.502 ± 0.124 | 0.454 ± 0.120 | 0.535 ± 0.110 |
| SAM($\epsilon$=0.05) | 0.688 ± 0.056 | 0.591 ± 0.071 | 0.526 ± 0.071 | 0.528 ± 0.071 | 0.526 ± 0.072 | 0.497 ± 0.071 | 0.509 ± 0.065 |
| RoMa | 0.944 ± 0.007 | 0.919 ± 0.015 | 0.882 ± 0.074 | 0.875 ± 0.049 | 0.786 ± 0.092 | 0.659 ± 0.139 | 0.713 ± 0.112 |

candidate image $x$ and compare it with the predefined signature $m$. The detection mechanism relies on testing the statistical hypothesis $H_1$: $x$ was generated by the watermarked model against the null hypothesis $H_0$: $x$ was not generated by the watermarked model. Specifically, they set a bit threshold $\tau$ and reject the null hypothesis $H_0$ when the number of matched bits $M(m, m')$ between the extracted message $m'$ and the signature $m$ satisfies:

$$M(m, m') \geq \tau \text{ where } \tau \in \{0, \ldots, k\}. \tag{3}$$

To obtain the False Positive Rate (FPR) associated with each bit threshold $\tau$, they assume the extracted bits follow an i.i.d. Bernoulli distribution with parameter 0.5 under $H_0$ (i.e., random guess between bit 0 and 1). This yields a binomial distribution for $M(m, m')$, with parameters $(k, 0.5)$. The FPR can then be formulated as:

$$\text{FPR}(\tau) = \mathbb{P}(M > \tau | H_0) = \sum_{i=\tau+1}^{k} \binom{k}{i} \frac{1}{2^k}. \tag{4}$$

## I. Experimental Setup for Stable Signature

Stable Signature (Fernandez et al., 2023) embeds watermarks into the Variational Autoencoder (VAE) decoder, so that all generated images carry binary messages. We follow the experimental settings of prior studies (Fernandez et al., 2023; Hu et al., 2024; Wang et al., 2024), and fine-tune the latent decoder to evaluate its robustness. Specifically, we use the MS-COCO-2017 validation set, randomly selecting 4,000 images for fine-tuning and reserving the remaining 1,000 images for evaluation. The fine-tuning process only minimizes the LPIPS loss between the original image and the image reconstructed by the latent decoder (as this maintains higher generation quality, following (Wang et al., 2024)), with a learning rate of $1 \times 10^{-4}$. For the watermarked model, we use the official checkpoint[7], which embeds a 48-bit binary message into the generated images. We set the bit threshold to $\tau = 38$ (FPR $= 10^{-6}$) for watermark detection.

## J. Experimental Setup for AquaLora

AquaLora (Feng et al., 2024) also embeds binary messages into all generated images. However, it differs in that it merges watermark information into the U-Net (Ronneberger et al., 2015; Ho et al., 2020; Rombach et al., 2022) using Low Rank Adaptation (LoRA) (Shen et al., 2022) through a scaling matrix strategy, thereby enabling watermark embedding during the denoising process. We evaluate the robustness of AquaLora against fine-tuning on the MS-COCO-2017 and CUB-200-2011 datasets, respectively, adopting the same fine-tuning protocol as described in the *Robustness Evaluation* section (Section 5.3). For the watermarked model, we first obtain the official prior-preserving fine-tuned checkpoints[8], and then embed the same 48-bit message as in Stable Signature into Stable Diffusion v1.5[9] with LoRA rank $= 320$. Here, we still set the bit threshold to $\tau = 38$ (FPR $= 10^{-6}$) for watermark detection (Fernandez et al., 2023; Wang et al., 2024). We use the prompt templates provided by AquaLora[10] for image generation, with the original Stable Diffusion v1.5 serving as the non-watermarked reference.

[7] https://github.com/facebookresearch/stable_signature
[8] https://huggingface.co/georgefen/AquaLoRA-Models/tree/main/ppft_trained
[9] https://huggingface.co/stable-diffusion-v1-5/stable-diffusion-v1-5/tree/main
[10] https://github.com/Georgefwt/AquaLoRA/tree/master/evaluation

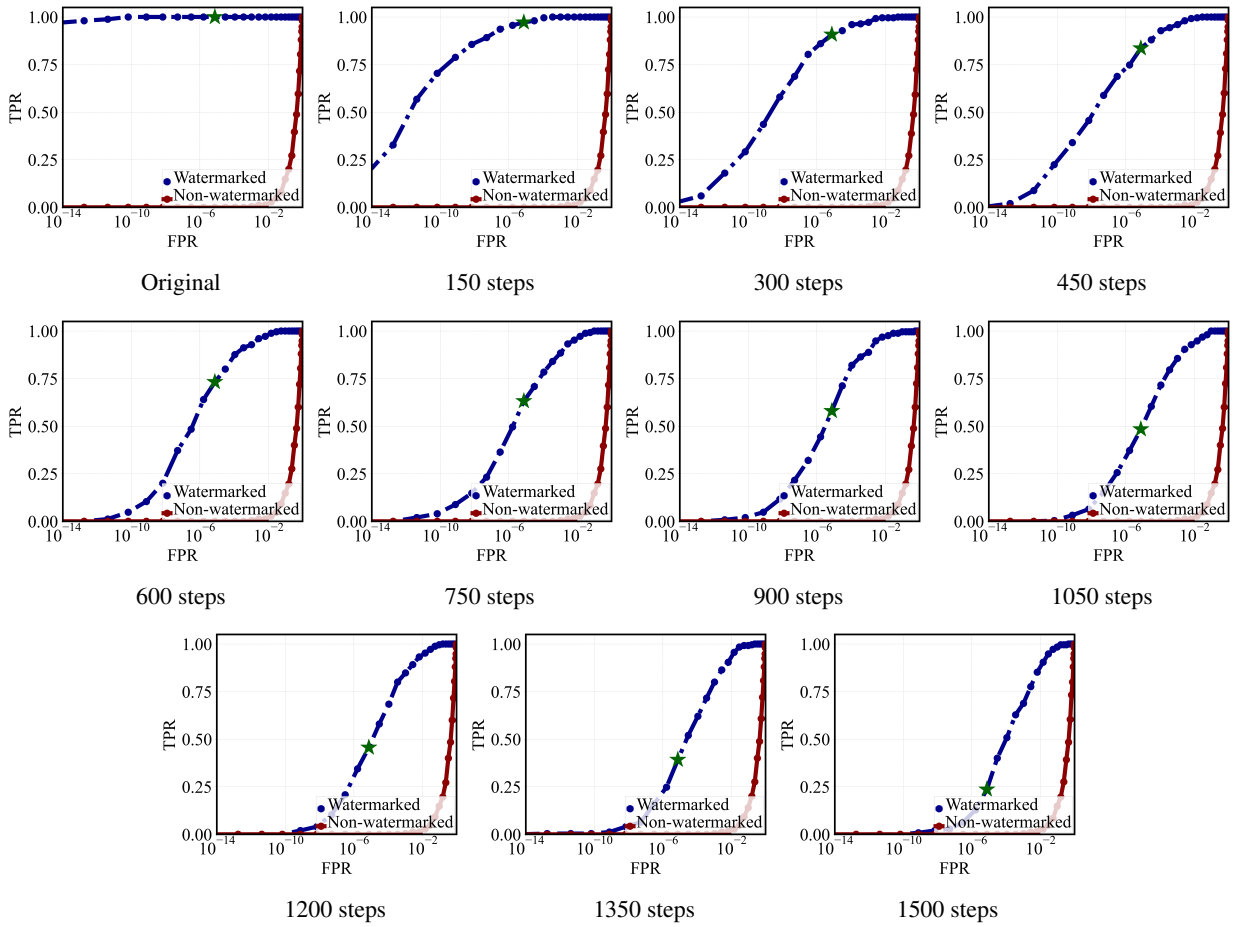


*Figure 14.* ROC curves of Stable Signature at various fine-tuning steps. The star with green color ($\star$) is highlighted (FPR $= 10^{-6}$) where its associated TPR reflects the detection accuracy with $\tau = 38$.

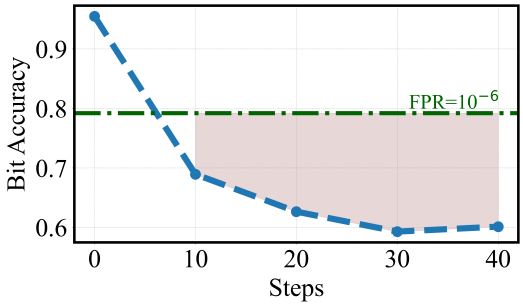


*Figure 15.* Bit accuracy results of AquaLora against the fine-tuning process on CUB-200-2011 dataset.

## K. Additional Discussions of Diffusion Models

Diffusion models (Ho et al., 2020; Nichol & Dhariwal, 2021; Ho & Salimans, 2022; Rombach et al., 2022; Podell et al., 2023; Song et al., 2020; Yang et al., 2023) have emerged as powerful generative paradigms, demonstrating remarkable success across various domains, including high-quality image synthesis (Dhariwal & Nichol, 2021; Ruiz et al., 2023; Zhang et al., 2023), video generation (Ho et al., 2022; Wu et al., 2023; Xing et al., 2024), and natural language generation (Lou et al., 2023). While our work focuses on protecting the watermarking robustness on Text-to-Image (T2I) diffusion models, our proposed RoMa is general and can be potentially adapted to watermarking diffusion models with different generative tasks (Lugmayr et al., 2022; Kawar et al., 2023), and architectures (Peebles & Xie, 2023).

*Figure 16.* Visual comparison between original images (top) and their reconstructions by Stable Signature's watermarked decoder (bottom).

*Figure 17.* Visual comparison between original images (top) and reconstructions by Stable Signature's watermarked decoder after 1500 fine-tuning steps (bottom).

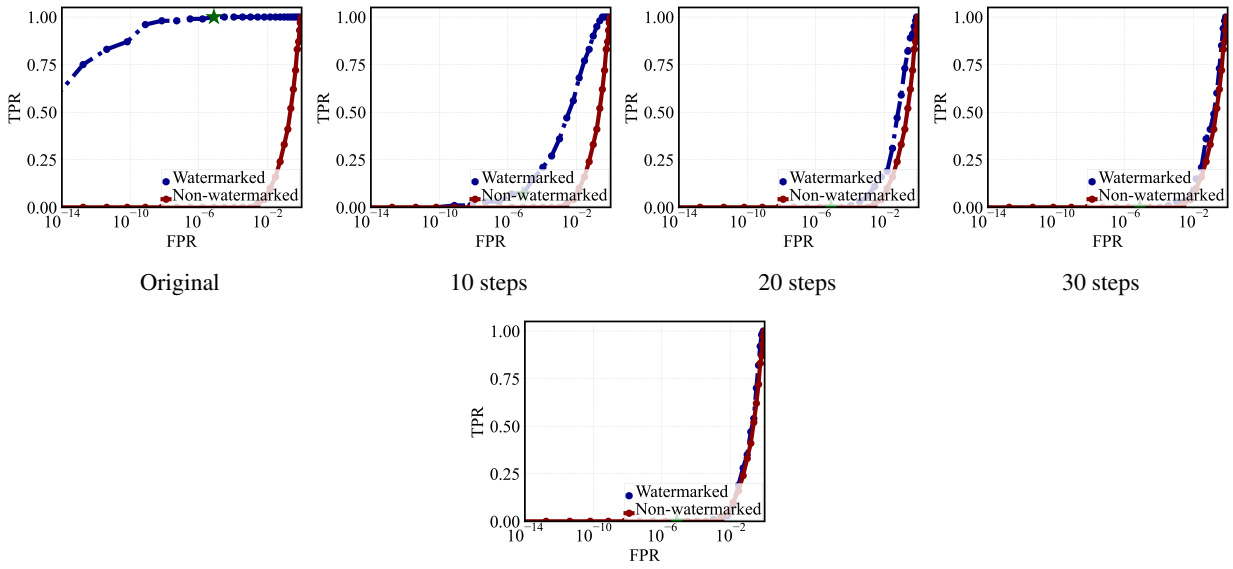


*Figure 18.* ROC curves of AquaLora at various fine-tuning steps on MS-COCO-2017 dataset. The star with green color ($\star$) is highlighted (FPR $= 10^{-6}$) where its associated TPR reflects the detection accuracy with $\tau = 38$.

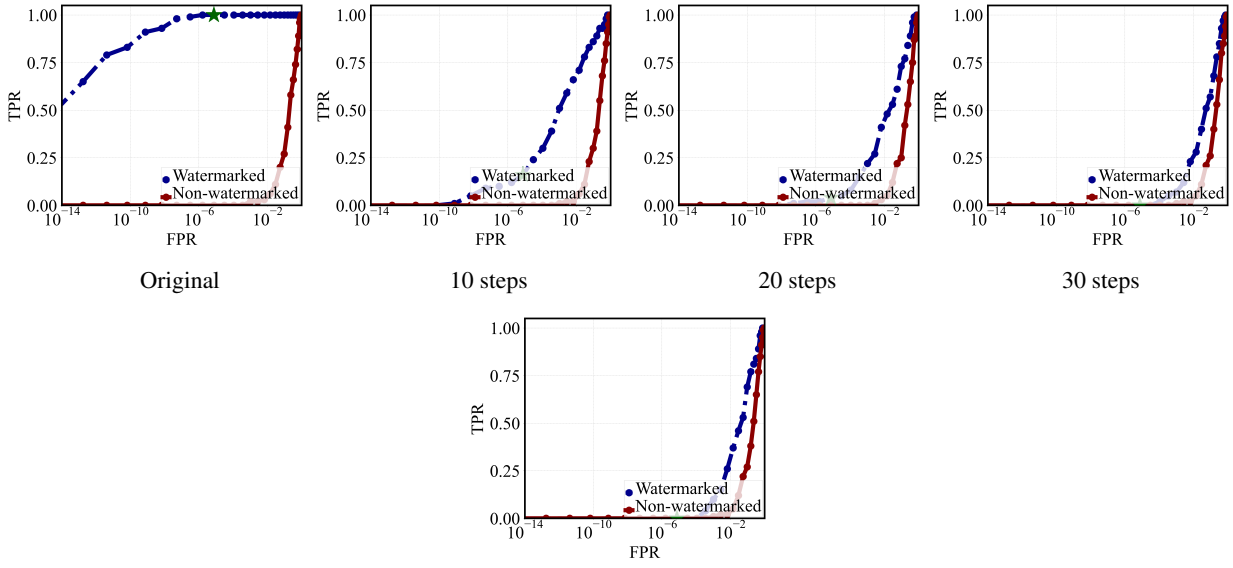


*Figure 19.* ROC curves of AquaLora at various fine-tuning steps on CUB-200-2011 dataset. The star with green color ($\star$) is highlighted (FPR $= 10^{-6}$) where its associated TPR reflects the detection accuracy with $\tau = 38$.